12-9-2006

Development and Validation of a Control Strategy for a Parallel Hybrid (Diesel-Electric) Powertrain

Jimmy C. Mathews

DEVELOPMENT AND VALIDATION OF A CONTROL STRATEGY FOR A PARALLEL HYBRID (DIESEL-ELECTRIC) POWERTRAIN

By

Jimmy Cherry Mathews

A Thesis
Submitted to the Faculty of
Mississippi State University
in Partial Fulfillment of the Requirements
for the Degree of Master of Science
in Electrical Engineering
in the Department of Electrical and Computer Engineering

Mississippi State, Mississippi

December 2006

DEVELOPMENT AND VALIDATION OF A CONTROL STRATEGY FOR A PARALLEL HYBRID (DIESEL-ELECTRIC) POWERTRAIN

By

Jimmy Cherry Mathews

Approved:

G. Marshall Molen Professor of Electrical and Computer Engineering (Director of Thesis)	Michael Mazzola Professor of Electrical and Computer Engineering (Committee Member)
Hossein Toghiani Associate Professor of Chemical Engineering (Committee Member)	Nicholas Younan Professor of Electrical and Computer Engineering (Graduate Coordinator)
Kirk Schulz Dean of the James Worth Bagley College of Engineering	

Name: Jimmy Cherry Mathews

Date of Degree: December 8, 2006

Institution: Mississippi State University

Major Field: Electrical Engineering

Major Professor: Dr. G. Marshall Molen

Title of Study: DEVELOPMENT AND VALIDATION OF A CONTROL STRATEGY FOR A PARALLEL HYBRID (DIESEL-ELECTRIC) POWERTRAIN

Pages in Study: 97

Candidate for Degree of Master of Science

The rise in powertrain complexity and the stringent performance requirements of a hybrid electric vehicle have elevated the role of its powertrain control strategy to considerable importance. Iterative modeling and simulation form an integral part of the control strategy design process and industry engineers rely on proprietary "legacy" models to rapidly develop and implement control strategies. However, others must initiate new algorithms and models in order to develop production-capable control systems. This thesis demonstrates the development and validation of a charge-sustaining control algorithm for a through-the-road parallel hybrid (diesel-electric) powertrain. Some approaches used in powertrain-level control of other similar vehicles have been adopted to incrementally develop this control strategy. The real-time performance of the control strategy has been analyzed through on-road and chassis dynamometer tests over standard drive cycles. Substantial quantitative improvements in overall performance over the stock vehicle, including better acceleration and fuel-economy have been achieved.

DEDICATION

You, O Lord, keep my lamp burning; my God turns my darkness into light.

The Bible, Psalms (ch. XVIII, v. 28)

I dedicate this work to The Almighty Lord and to my beloved parents, for their unconditional love and everlasting support.

ACKNOWLEDGMENTS

Challenge X (cX) is undoubtedly the crescendo of my academic stint at Mississippi State University (MSU). At the very outset, I express my sincere gratitude to Dr. G. Marshall Molen, my major professor and the cX faculty advisor for having deemed me worthy to work on this prestigious project. He has been an unswerving source of advice, support and constructive criticism in the course of my work on cX.

I am indebted to Dr. Michael Mazzola for initiating me to this project. I thank him and Dr. Hossein Toghiani for gladly agreeing to serve on my graduate committee.

This work is the culmination of several technical ideas and suggestions spanning across several domains. I have been fortunate to be associated with a fine group of well-read and light-hearted colleagues in David Oglesby, Kennabec Walp, Christopher Whitt and Kyle Crawford. I am a more knowledgeable person due to my constant and wide-ranging interactions with them and all the other members of the MSU cX team.

Finally, I acknowledge the support received from the primary funding sources for this project – the Center for Advanced Vehicular Systems at MSU, the James Worth Bagley College of Engineering at MSU, the U.S. Department of Energy (Argonne National Laboratory) and the General Motors Corporation.

TABLE OF CONTENTS

CHAPTER Page

LIST OF TABLES

LIST OF FIGURES

FIGURE Page

FIGURE Page

FIGURE Page

FIGURE Page

LIST OF SYMBOLS

AT	Automatic transmission
BMS	Battery management system
C	Capacity of the NiMh battery pack
C_P	Specific heat of a gas at constant pressure
C_V	Specific heat of a gas at constant volume
CIDI	Compression ignition direct injection
CO	Carbon monoxide
cX	Challenge X
d	Distance traveled
DPF	Diesel particulate filter
E_{B20}	Energy content of B20 bio-diesel
E_{CUM}	Cumulative value of energy content of fossil fuel used by the HEV ($E_{IN} + E_{OUT}$)
E_{IN}	Electrical energy into the battery
E_{OUT}	Fossil fuel i.e. B20 energy out of the fuel tank
E_{RFG}	Energy content of reformulated gasoline (RFG)
ECU	Electronic control unit
EM	Electric machine
EPA	Environmental Protection Agency

FCV	Fuel-cell powered vehicle
FTP	Federal Test Procedure
GE	Gasoline equivalent
HC	Hydrocarbons
HEV	Hybrid electric vehicle
HV	High voltage
HWFET	Highway fuel economy test
ICE	Internal combustion engine
IVM	Initial vehicle movement
k	Ratio of specific heats
k_1, k_2	Constants based on torque coupling
MAAB	Matlab Automotive Advisory Board
MC	Motor controller
MT	Manual transmission
NiMH	Nickel metal hydride
NO_X	Nitrous oxides
NREL	National Renewable Energy Laboratory
OEM	Original equipment manufacturer
P	Fixed ratio of the rear wheel reducer
PM	Particulate matter
PSAT	Powertrain System Analysis Toolkit™
PSC	Powertrain system controller

R	Transmission gear ratio
RBS	Regenerative braking system
RFG	Reformulated gasoline
RT	Real-time
SCR	Selective catalytic reduction
SFTP	Supplemental Federal Test Procedure
SOC	State of charge of the battery
t	Sample time
T_{EM}	Torque contribution of the electric machine
T_{ICE}	Torque contribution of the engine
T_{WH}	Torque output at the wheels
TTR	Through-the-road
UDDS	Urban dynamometer driving schedule
V_{NOCV}	Nominal open circuit voltage of the battery pack
V_{OC}	Open circuit voltage of battery
WOT	Wide open throttle
β	Initial SOC of the battery (%)
γ	Amount of B20 fuel used
ε	Compression ratio of the engine
η_{CON}	Cumulative conversion efficiency
η_{gb}	Efficiency of the gear box
η_{ICE}	Theoretical efficiency of the engine

η_{red}	Efficiency of the reducer
λ	Final SOC of the battery pack (%)
ω_{EM}	Speed of the electric machine
ω_{ICE}	Speed of the engine
ω_{WH}	Speed at the wheels
ΔSOC	Change in SOC of the battery pack

CHAPTER 1

INTRODUCTION

Concerns about the environment and the depletion of fossil fuel resources have promoted widespread interest in the adoption of alternative technologies for transportation. In light of the glaring disadvantages of conventional gasoline and diesel-fueled vehicles, primarily because of the inefficient use of petroleum and the exhaust emissions, automotive manufacturers have been forced to explore other concepts. Internal combustion engine (ICE)-based hybrid electric vehicles (HEV) and fuel-cell powered vehicles (FCV) have acquired considerable attention as alternative vehicle propulsion technologies. However, HEVs employing the mature engine technology have currently gained greater acceptability than FCVs in the automotive industry and market, primarily because of the challenges posed by the use of hydrogen.

1.1 Internal Combustion Engine-powered Hybrid Electric Drivetrains

Hybrid vehicles utilize combinations of two or more power sources in a variety of powertrain architectures to achieve vehicle propulsion. Typically, a hybrid vehicle is equipped with two power sources, most often an engine and an electric machine (EM). An HEV will possess energy storage capability such as a battery pack or an ultracapacitor, which along with the electric machine and power conditioning devices form the electrical subsystem of the powertrain. With the introduction of additional

power sources and the ensuing rise in powertrain complexity, the control system in an HEV is elevated to a role of considerable importance. Figure 1.1 shows a conceptual illustration of an HEV drivetrain.

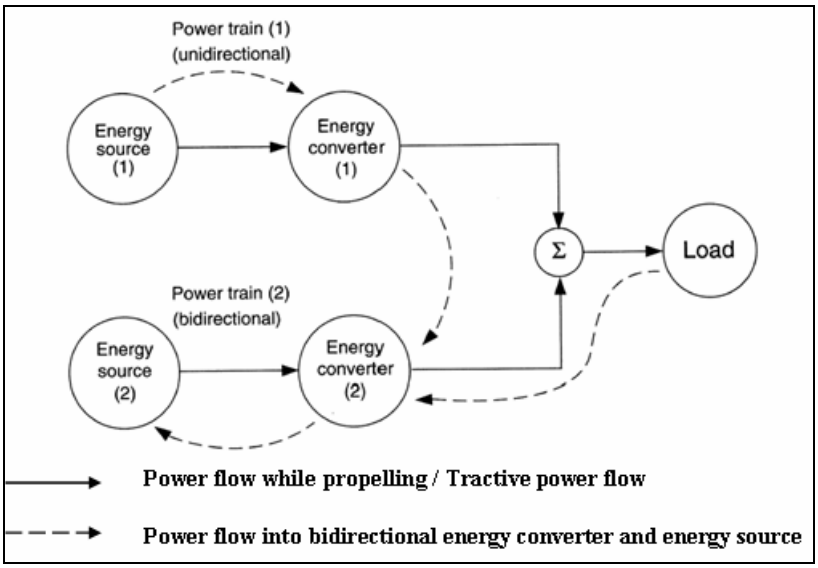

Figure 1.1: Conceptual Illustration of a Hybrid Electric Drivetrain [1]

HEV drivetrains can be classified based upon the arrangement of the propulsion sources (series, parallel, series-parallel or complex), or upon the manner in which power from the sources is added (torque-combination or speed-combination) or depending upon the degree of hybridization (micro, mild, full, plug-in or muscle) [2, 3]. While traditional classifications of engine-powered hybrid drivetrains include series and parallel hybrids, many new HEV configurations fall under the category of series-parallel and complex hybrids. Figure 1.2 illustrates some hybridization options between a conventional and an electric automobile. The split-hybrid is a series-parallel hybrid where the engine power can be transformed through the electric machine into electric power or it may be directly

transmitted to the drive axle. The through-the-road (TTR) hybrid has been very suitable as a power hybrid in 4-wheel drive applications [4].

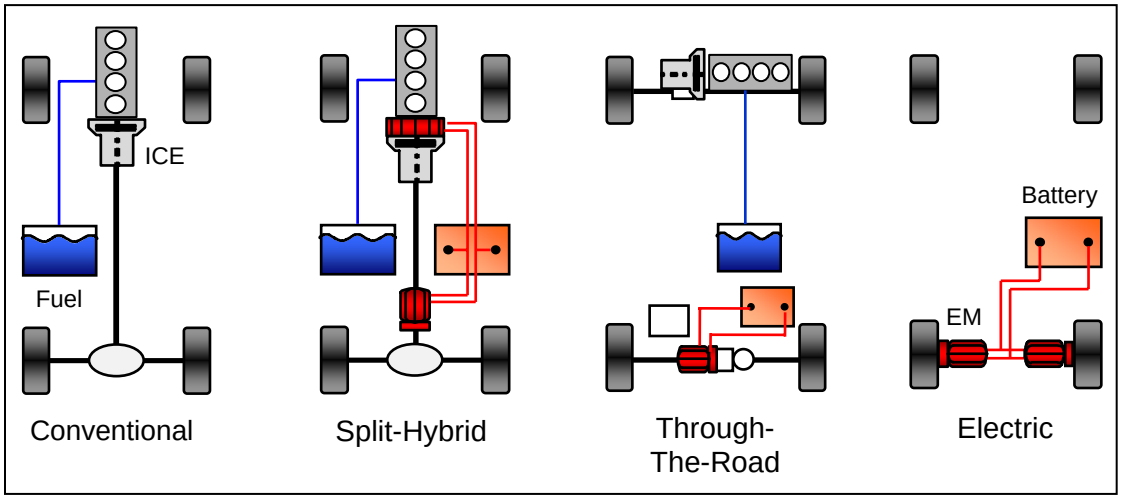

Figure 1.2: The Hybrid – An Evolution between Conventional and Electric Vehicles [4]

Figure 1.3 provides a classification of hybrid drivetrains based on the features employed. An addition to this checklist is a 'micro-hybrid' which does not provide any power for propulsion but augments the engine operation by supplying power for restarting the engine via a stop-start capability. Micro-hybrids are also capable of regenerative braking. Among the recent popular hybrids, the Honda Insight and Honda Civic Hybrid are mild hybrids while the Toyota Prius is a full hybrid [5, 6]. The following discussion focuses mainly on parallel hybrid powertrains and their variants.

1.2 Parallel Hybrid Electric Drivetrains

In a parallel HEV, the engine supplies power to the wheels through a mechanical transmission path just like in a conventional vehicle. Typically, the electric machine

assists the engine and these power sources are coupled by a mechanical coupling. Figure 1.4 illustrates a generic configuration of a parallel hybrid powertrain. The engine and electric machine are combined either by torque-coupling, speed-coupling or both [1, 7].

Does this vehicle...	Conventional Vehicle	Muscle Hybrid	Mild Hybrid	Full Hybrid	Plug-in Hybrid
Shut off the engine at stop-lights and in stop-and-go traffic	✓	✓	✓	✓	✓
Use regenerative braking and operate above 60 volts		✓	✓	✓	✓
Use a smaller engine than a conventional version with the same performance			✓	✓	✓
Drive using only electric power				✓	✓
Recharge batteries from the power grid and have an electric-only range of at least 20 miles.					✓

Figure 1.3: Hybrid Drivetrain Classification by Degree of Hybridization [5]

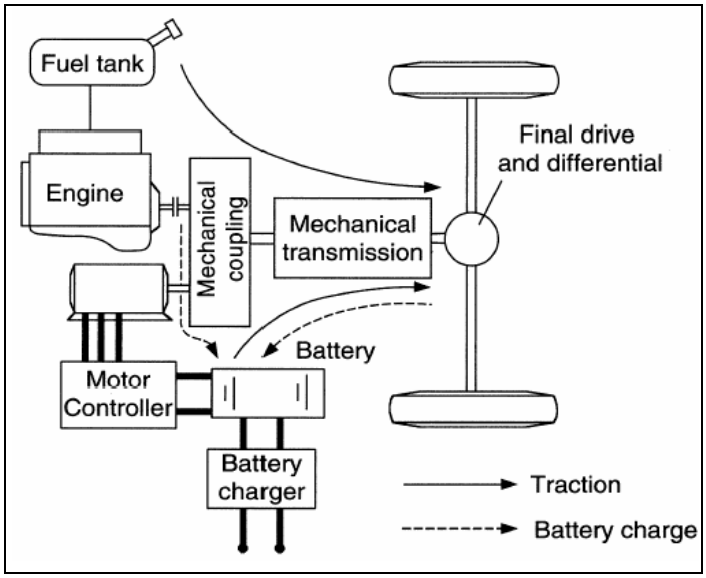

Figure 1.4: Configuration of a Parallel Hybrid Drivetrain [1]

In a torque-coupling scheme, the torques of the engine and the electric machine (functioning as a motor) are either added together or the engine torque is split into torque required for propulsion and battery charging. The speeds of the engine and the electric machine share a predetermined relationship with the vehicle speed. For a mechanical torque coupling with the two inputs from the engine and the electric machine, the output torque and speed (i.e. torque and speed at the wheels) are described as follows [1].

$$T_{WH} = k_1 \times T_{ICE} + k_2 \times T_{EM} \tag{1}$$

$$\omega_{WH} = \frac{\omega_{ICE}}{k_1} = \frac{\omega_{EM}}{k_2} \tag{2}$$

T_{ICE} and T_{EM} are the torque contributions of the engine and the electric machine respectively, while ω_{ICE} and ω_{EM} are the speeds associated with them. The constants k_1 and k_2 are determined by the parameters of the torque coupling and depend on the specifics of the mechanical coupling system.

Parallel hybrid drivetrains of the torque combination type may further be classified into single-shaft and two-shaft configurations. The transmissions in these cases could be either single or multi gear depending on the desired tractive torque-speed profile. In a single-shaft arrangement where only one transmission is used, the transmission may be placed either behind the electric machine or between the engine and the electric machine. These configurations are referred to as pre-transmission and post-transmission, respectively. The family of torque-coupled parallel drivetrains also includes a separated-axle architecture which is the focus of attention in this thesis [1, 7].

1.3 The MSU cX Vehicle Architecture – Design Concept and Description

The powertrain considered in this thesis is the Mississippi State University (MSU) Challenge X (cX) team's TTR parallel HEV. Challenge X is a three-year, vehicle design competition in which seventeen engineering schools across North America were asked to re-engineer a 2005 Chevrolet Equinox to make it more efficient and less exhaust emitting, while maintaining or exceeding the stock vehicle performance. The separated-axle, double-shaft drive architecture of the TTR parallel powertrain is depicted in Figure 1.5.

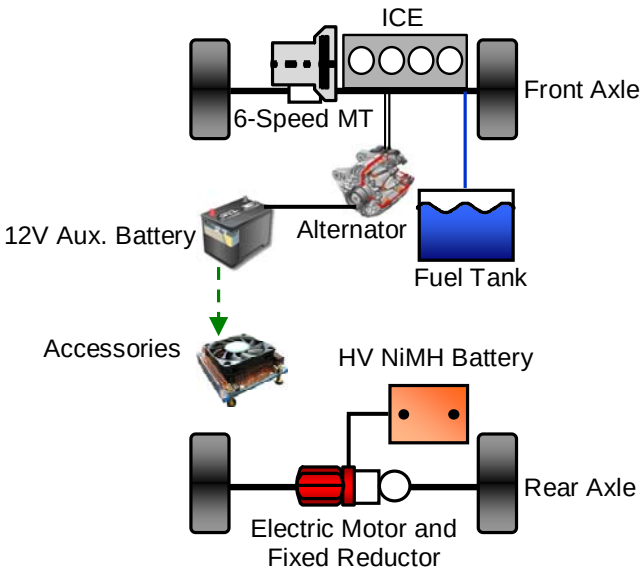

Figure 1.5: Architecture of a Through-The-Road Parallel Powertrain as Adapted for the MSU cX Competition Vehicle [8]

The TTR parallel concept is simple in construction because the engine and the electric machine are not physically connected to each other. Rather, each of them drives a different pair of wheels with the required propulsion power (torque) combined 'through-the-road'. This is also akin to the vehicle body serving as a torque summing device [1, 9].

A benefit of this concept is the flexibility of driving the two pairs of wheels, either selectively in two-wheel drive or simultaneously in four-wheel drive. This feature provides the vehicle with operation flexibility and redundant drive system capability through a limp-home mode of operation [10]. With the engine driving the front axle and the electric machine driving the rear axle in the MSU cX design configuration (or vice versa, if desired), the combined sources can provide enhanced thrust when maximum torque is required. The electric drive can be connected through either a single or a multi gear and provides the HEV powertrain with electric-boost during periods of sudden and high torque requirement [11].

In the vehicle braking mode, the electric machine can function as a generator and recharge the battery. Additionally, when the battery state-of-charge (SOC) falls below a stipulated minimum level, the engine can perform the dual tasks of propelling the vehicle and recharging the battery to at least a minimum SOC. Most of the energy for charging the battery is recovered during braking. The efficiency-enhancing regenerative braking system (RBS) is integrated with the hydraulic friction brakes to provide for maximum braking reliability and regenerative energy capability. It must be noted that the battery cannot be charged by the engine when the vehicle is at standstill since there is no power flow path from the engine to the high voltage (HV) electrical subsystem [1].

Ideally, a powertrain controller that optimizes the operation of all the major vehicle components is required to maintain a delicate balance between the fuel economy, emissions and driveability considerations of the HEV. Table 1.1 lists the components selected for the MSU hybrid vehicle along with their technical specifications.

Table 1.1: Component Technical Specifications for the MSU TTR Parallel HEV [8]

Component	Specification
IC Engine	1.9 L, 109 kW, Fiat/GM CI engine
Electric Motor	Ballard Ranger AC induction drive with 67 kW peak and 32 kW continuous power rating, 12.52:1 transaxle assembly
Battery Pack	Johnson Controls NiMH battery pack with 330 V, 7 A-h capacity, 44 modules with 6 cells/module
Transmission	6-speed GM manual transmission with a final drive ratio of 3.545

1.4 Thesis Contribution and Organization

The goal of this thesis is to develop and validate a charge-sustaining control algorithm for a TTR parallel HEV. A control algorithm is a set of rules that govern the operation of the powertrain. Based on operation commands from the driver and feedback from the components, the control algorithm makes decisions on operating modes by controlling (increasing, reducing or maintaining) component power outputs or by switching components on/off.

The heart of an HEV is its main controller, also known as the Powertrain System Controller (PSC). The PSC performs a supervisory function of optimally distributing the driver-requested power among the available sources. The PSC acts like an interpreter between the man-machine interface, i.e. the driver and the powertrain. In a typical engine-powered hybrid powertrain, the PSC issues appropriate power (torque) requests to the engine and electric machine based upon the logic specified through a control

algorithm. Constant monitoring of the driver's demands and detection of existing and possible fault scenarios are expected to be inherent functions of the PSC. The control algorithm for an HEV has attained utmost importance due to the complexity of vehicle configurations, the need to ensure smooth transitions between various modes of operation and constant attempts to maximize the efficiency of the powertrain.

The organization of this thesis is as follows. Chapter 2 gives an overview of the control problem specific to the MSU powertrain. Chapter 3 discusses the actual development of the control algorithm for the TTR parallel powertrain and the state machine logic adopted within the algorithm. Chapter 4 presents some performance predictions obtained through simulation, and analyzes the on-road and chassis dynamometer test results. The thesis concludes with a summary of the implementation together with a suggestion of improvements that may be made in the future.

CHAPTER 2

CONTROL STRATEGIES FOR HYBRID ELECTRIC VEHICLES

2.1 Overview of Control of Series and Parallel Hybrid Powertrains

There is a fundamental difference in the overall control of series and parallel hybrid powertrains, especially in engine-dominated HEVs. In a series powertrain, the actual propulsion occurs due to a traction motor coupled to the drive wheels while the engine-generator system is mechanically decoupled from the drive wheels of the HEV. The torque request to the electric machine is calculated by dividing the torque demand at the wheels by the total gear ratio and is bounded by the maximum limits of the electrical subsystem. Optimal operation of a series configuration therefore depends on how the engine load is managed. The speed and torque of the engine are independent of the vehicle speed and driver demand for traction torque. Hence to optimize engine efficiency, the speed and torque at any instance can be controlled to operate at virtually any point on its speed vs. torque plane [12, 13].

In a series powertrain, the engine can be operated in one of the following three different modes [13].

- At the maximum efficiency point corresponding to a specific speed and torque
- Along the optimal efficiency curve
- Along the maximum torque curve

Selection of one of the three modes is based on the power (speed × torque) demand from the engine. If the power required from the engine is less than the power available at the maximum efficiency point, the engine is operated at this point. The points I, II and III illustrated in Figure 2.1 are characterized by the property that they correspond to a lower efficiency than theoretically achievable by the engine. These operating points can be shifted closer to the point of best efficiency by controlling the speed and torque of the engine. While the power output of the engine will also change, this is an overall control issue and is accounted for by using the battery to balance the difference in engine power. The maximum efficiency point operating mode is not employed if the battery capacity is small since the battery may be easily overcharged [12, 13].

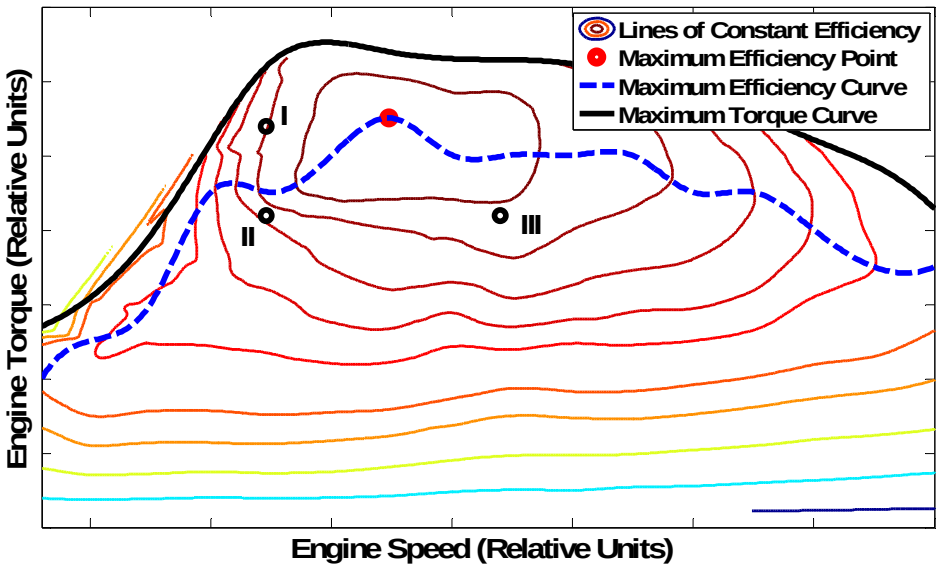

Figure 2.1: Generic Efficiency Map of an Engine with Location of Arbitrary Operating Points Relative to the Point of Best Efficiency.

If the engine power demand is greater than the power available at the maximum efficiency point, the engine is operated along the optimal efficiency curve. From the optimal engine efficiency curve and the engine power demand, the corresponding torque and speed are calculated. However, if no point on the optimal curve satisfies the power demanded from the engine, the engine is operated on the maximum torque curve [13].

In a parallel torque-coupled hybrid powertrain, the engine is mechanically coupled to the drive wheels and hence the speed of the engine is imposed by the vehicle speed based upon the transmission gear ratio. The control system designer has more control over the engine torque than the engine speed [12]. Hence, the maximum efficiency point strategy, as applicable for the control of the engine in series hybrid powertrains is not a viable option for parallel hybrids due to the restriction on control of the engine speed.

In a parallel configuration the engine is expected to operate over a wide range of speeds and loads and hence cannot be constrained to a particular optimum efficiency or emissions point [13]. However, it is possible to operate the engine on the optimal efficiency curve. Engine load balancing is performed by the bidirectional electrical subsystem of the powertrain consisting of the electric machine and the energy storage device. Figure 2.2 shows the operating points I and II that are shifted onto the engine optimal efficiency curve by manipulation of the torque output level.

A number of control strategies have been proposed and implemented for control of parallel hybrid powertrains. Ehsani, Gao, Gay and Emadi [1], Liang, et al. [14] and, Buntin and Howze [15] proposed control schemes aimed at optimizing the battery SOC.

These were called as ‘Maximum/Best Battery SOC’ or ‘Maximum Vehicle Range’ control. The ‘Thermostat’ or ‘On/Off’ or ‘Bang-Bang’ control is another control technique. It was developed initially for a series hybrid drivetrain and was later extended to the power flow control in a parallel HEV [1, 16, 17, 18]. The engine load-leveling control algorithm is arguably the most popular power distribution algorithm for control of parallel hybrid powertrains. The idea of load-leveling is to force the engine to act at or near its peak point of efficiency or its best fuel use at all times [12, 19].

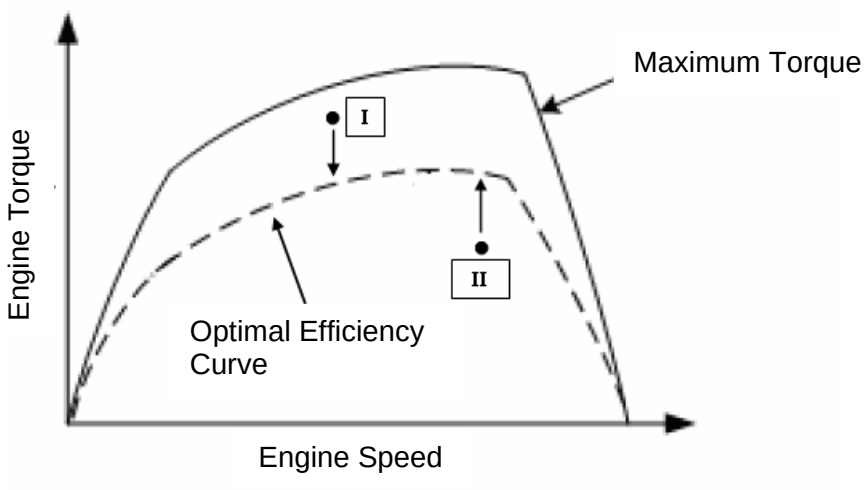

Figure 2.2: Engine Torque Curves and Torque-based Manipulation of Operating Points

2.2 Overview of the Drive Control Problem for the TTR Parallel HEV

Prior to exploring options for the MSU HEV control strategy, it is essential to define the mechanical relationships that govern the operation of the parallel hybrid powertrain. This is especially significant because, although the different powertrain components operate concurrently, they need to be controlled individually. Valid

operating ranges of the parallel double-shaft arrangement of the HEV are defined. A representative arrangement of the selected powertrain is shown in Figure 2.3. Since the mechanical arrangement of the powertrain is of a torque-summation type, the control variables that are manipulated to achieve appropriate driving force distribution between the engine and the electric machine are the torques produced by the respective power sources. The speeds of these power sources are imposed by the instantaneous vehicle speed at different mechanical reduction ratios.

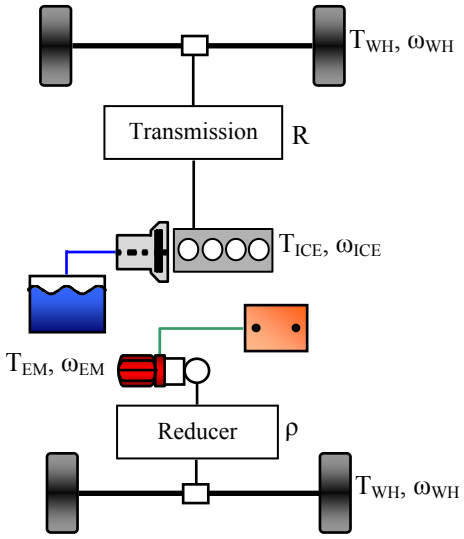

Figure 2.3: Representation of Mechanical Arrangement of the TTR Parallel HEV [8]

For this mechanical arrangement, the speed and torque at the wheels are given by:

$$T_{WH}(t) = [R(t) \times \eta_{gb} \times T_{ICE}(t)] + [\rho \times \eta_{red} \times T_{EM}(t)] \tag{3}$$

$$\omega_{WH}(t) = \frac{\omega_{ICE}(t)}{R(k(t))} = \frac{\omega_{EM}(t)}{\rho} \tag{4}$$

In the above equations R is the transmission gear ratio, η_{gb} and η_{red} are the efficiencies of the gearbox and the reducer. Mechanical constraints limit the torque and speed of the MSU powertrain configuration. It should be noted that the engine provides only positive torque while the torque provided by the electric machine may be either positive or negative. The torque sign of the electric machine is a major factor for ensuring charge-sustainability of the HEV. The ratio of the rear wheel reducer (ρ) is a constant that is influenced by trade-offs between the maximum allowable vehicle speed and maximum torque at low speeds.

2.3 Control Strategy for the Georgia Tech Split-Parallel Hybrid Electric FutureTruck

This section discusses a control strategy that was developed and implemented for a parallel hybrid powertrain. The control strategy was utilized by a student group at the Georgia Institute of Technology for their HEV in the FutureTruck competition [20, 21]. The HEV is a strong, split-parallel hybrid powertrain where a 3.0 L, V6, 157 kW Lincoln LS gasoline engine drives the rear wheels and a 150 kW AC induction machine with a peak torque of 220 N-m is coupled to the front differential through a 53:23 fixed ratio speed reducer. In this context, the term ‘strong’ refers to a configuration where the power of the electric machine is approximately 50% of the cumulative engine and electric machine power. The engine drives the rear axle differential through a 5-speed automatic transmission (AT). The powertrain includes a 336 V, 16 A-h lead acid battery. This configuration is similar to the MSU HEV except that different power sources drive the front and rear axles [20, 21].

In the Georgia Tech HEV, a cable connection has been maintained between the accelerator pedal and the engine throttle. This has been done primarily for safety considerations to prevent the driver accelerator pedal request from being overridden. The presence of this cable prevents any drive-by-wire throttle control by the engine electronic control unit (ECU). Engine idle-off is not a part of the control strategy. The controller uses the accelerator pedal position, the brake pedal position, battery SOC and vehicle speed to compute the torque command to the electric machine [20].

During normal acceleration of the HEV from low vehicle speeds, the electric machine responds to the accelerator pedal position by providing most of the accelerating torque. At low battery SOCs, the driver must further depress the accelerator pedal so as to request more torque from the engine. With an increase in vehicle speeds, the engine contributes a major portion of the traction torque as compared to the electric machine. During wide open throttle (WOT) - also called high-performance acceleration - both the engine and the electric machine provide the maximum available torques. Cruising at normal speeds is characterized by battery charging at very low magnitudes, while the engine responds to the accelerator pedal request. When the accelerator pedal is released and the brake pedal is touched in its free-play at the top, the engine idles and the electric machine regenerates. Regeneration is employed in a gradually decreasing manner with the hydraulic friction brakes engaging at a later point of brake pedal travel. A reduction in vehicle speed reduces the contribution of the electric machine for braking, thus necessitating the driver to further depress the brake pedal and engage the normal friction brakes [20].

It is interesting to note that the power ratings of the engine and the electric machine in the Georgia Tech HEV are greater than those in the MSU HEV. Moreover, a gasoline engine is used as opposed to a diesel engine in the MSU HEV. The control algorithm of the Georgia Tech HEV employs continuous plots of the motor controller (MC) input voltage vs. accelerator pedal position for different battery SOCs and at vehicle speeds in order to determine the torque request to the electric machine [20]. These plots form the initial bases for the development of a control strategy for the MSU HEV.

CHAPTER 3

CONTROL ALGORITHM DEVELOPMENT FOR A THROUGH-THE-ROAD PARALLEL HYBRID ELECTRIC VEHICLE

3.1 Criteria for Optimization (Trade-offs) for the HEV Control Algorithm

In a conventional vehicle, the engine load points (speed and torque combinations) that fulfill the instantaneous tractive power demand are chosen and hence the engine does not necessarily operate at high efficiency at all times. This is especially noticeable at low loads. Also, load transients adversely affect the emissions because of sudden increases in injected fuel. Conventional vehicles like the stock 2005 Chevrolet Equinox possess reserve engine power capabilities that are seldom utilized. This is where engine downsizing and the use of diesel engines are beneficial to some extent [22].

Downsizing the engine allows it to be operated close to its peak fuel efficiency or low specific fuel consumption rates. The stock 138 kW gasoline engine (138 kW @ 5200 r/min, 285 N-m @ 3800 r/min) was downsized to a 109 kW, 1.9 L GM diesel engine (109 kW @ 4000 r/min, 320 N-m @ 2000 r/min) in the MSU HEV powertrain [23, 24]. Diesel engines have higher maximum efficiencies than their gasoline counterparts and this is generally attributed to higher compression ratios (approximately 18:1 in the MSU diesel engine). The theoretical efficiency of an engine (η_{ICE}) is given by [22]:

$$\eta_{ICE} = 1 - \frac{1}{\varepsilon^{k-1}} \tag{5}$$

Here ε is the compression ratio of the engine, k is the ratio of specific heats (C_P/C_V), C_P is the specific heat of a gas at constant pressure and C_V is the specific heat of a gas at constant volume. The compression ratio of an engine is limited by friction losses, but that aspect will not be discussed here. The high theoretical efficiency of the diesel engine contributes to better utilization of the available fuel as compared to a gasoline engine. Engine efficiency is the greatest at higher torques and mid-range rotational speeds [22].

From a controls perspective, the design objectives for the MSU HEV are to achieve low overall fuel consumption while maintaining battery charge-sustainability over standard driving schedules. This is significant since the development of a control algorithm needs to address specific issues that may involve trade-offs with other simultaneous improvements. A case in point is the trade-off between high engine efficiency and low emissions in a diesel engine. On the torque-speed map of a diesel engine, the loci of maximum efficiency points may not necessarily correspond to the loci of lowest emissions. For a diesel engine, the four regulated emissions are hydrocarbons (HC), carbon monoxide (CO), nitrous oxides (NO_X) and particulate matter (PM). The dominant drawbacks with diesel engines are the high NO_X and particulate matter emissions [22].

Figure 3.1 illustrates four distinct regions of optimization for a generic compression ignition direct injection (CIDI) engine. There is an evident trade-off between all the four possible improvements. Thus control algorithms for HEVs cannot merely account for the general power flow but they also have to simultaneously balance and select among the contrasting low emissions and high efficiency load points.

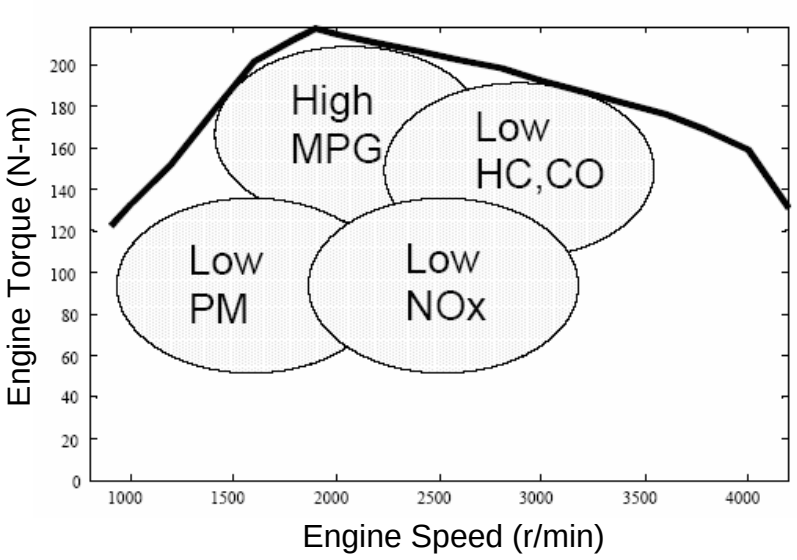

Figure 3.1: Fuel Economy and Emissions Tradeoffs for a Generic CIDI Engine [25]

Figures 3.2 and 3.3 illustrate the engine efficiency and the instantaneous fuel flow rate, respectively, for the entire range of load points for the 1.9 L GM diesel engine. Figure 3.4 shows the measured NO_X emissions (g/min). The operating load points for the GM diesel engine are likely to be different for each optimization goal. An engine efficiency-optimized control algorithm may cause the engine to operate in regions of high NO_X emissions. When the control algorithm optimizes for high engine efficiency, the fuel consumption of the engine is expected to reduce. However, there is a difference in optimizing for high engine efficiency and optimizing for low overall fuel consumption. In the former case, the engine may be forced to operate at a higher efficiency or be switched off at a certain efficiency level and the electrical subsystem is made to account for the variations in power requirement. But high efficiency does not necessarily imply low fuel consumption at the end of the drive cycle. It could so happen that although the engine

may be operating at a high efficiency, the electric machine and its associated electrical subsystem may be ruining the savings in fuel consumption through electrical power losses. This might cause low overall system efficiency and thereby lead to insignificant or no gains in overall fuel consumption [22].

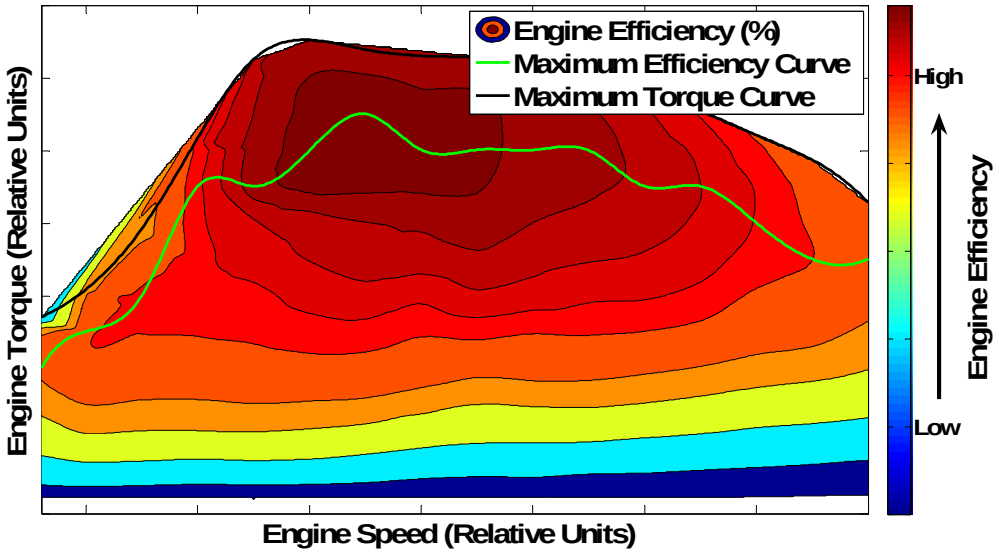

Figure 3.2: Efficiency Map of the 1.9 L GM Diesel Engine [24]

From Figures 3.3 and 3.4, it can be seen that low instantaneous fuel flow rate and low NO_X emissions share a region of significant overlap for the 1.9 L GM diesel engine. Hence rather than optimizing for engine efficiency, a relatively simple, but effective approach for the present work is to optimize for low instantaneous fuel flow rate to the engine. This approach will simultaneously optimize for low NO_X emissions. Emissions in the MSU HEV are also "controlled" by the urea selective catalytic reduction (SCR) system for NO_X emissions and the diesel particulate filter (DPF) for particulate matter, the study of which is beyond the scope of this thesis.

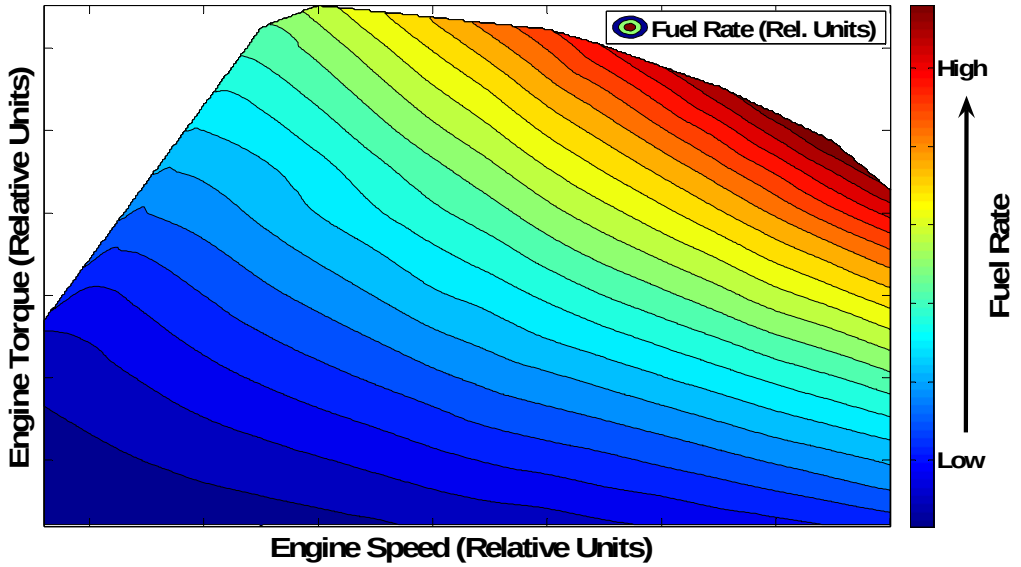

Figure 3.3: Instantaneous Fuel Flow Rate of the 1.9 L GM Diesel Engine [24]

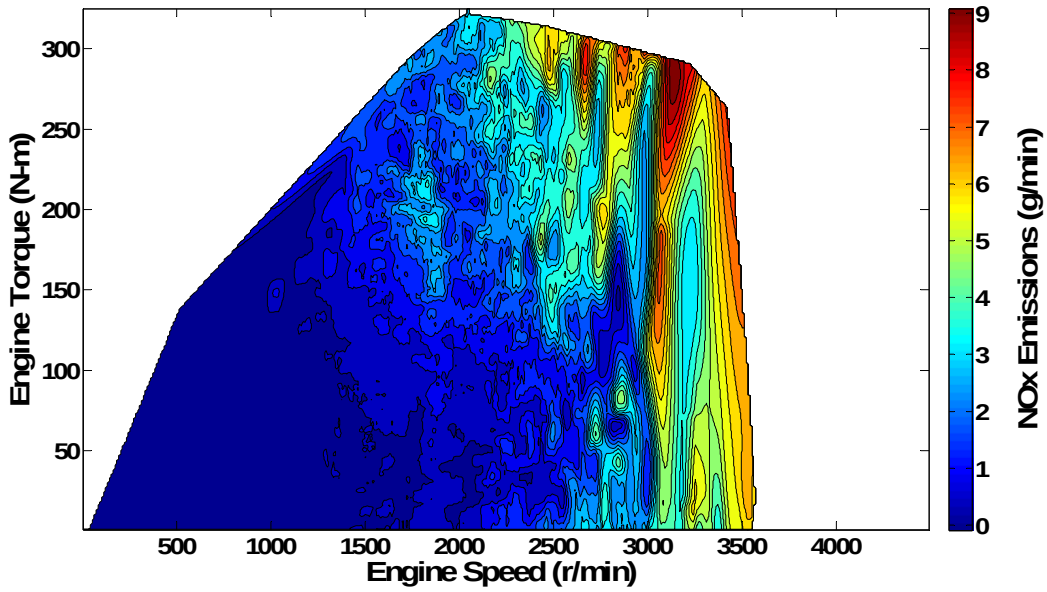

Figure 3.4: Measured NO_X Emissions (g/min) for the 1.9 L GM Diesel Engine

3.2 Objectives of the Control Algorithm and Minimum Targets

Table 3.1 shows the dynamic performance parameters of the stock 2005 Chevrolet Equinox. The targets for the MSU HEV are to improve or at least maintain the stock vehicle performance.

Table 3.1: Important Performance Parameters of the Stock 2005 Chevrolet Equinox [23]

Category Description	Stock Equinox Performance
0 – 60 mi/h Acceleration	8.5 s
50 – 70 mi/h Acceleration	6.3 s
Fuel Economy – UDDS (mi/gal)	19 mi/gal
Fuel Economy – HWFET (mi/gal)	25 mi/gal
Trailer Towing Capacity (at 55 mi/h and 7% road grade)	1588 kg

The prime design objectives of the MSU HEV control algorithm are:

1. Consistently satisfy driver inputs while meeting performance requirements such as acceleration, gradeability and cruising speeds.
2. Achieve low overall fuel consumption as compared to the stock gasoline and diesel-only configurations.
3. Provide charge-sustainability so as to maintain the battery SOC at reasonable levels without the necessity of charging from an external source
4. Recover maximum regenerative braking energy
5. Attempt to lower NO_X emissions

3.3 Design Approach for the MSU TTR Parallel Control Strategy

In order to ensure that the driver demands are always met, the torque required is split into individual torque requests, to the engine and the electric machine by the PSC based on the vehicle operating mode. Figure 3.5 depicts the hierarchy of controllers in the MSU HEV. The Motorola MPC555 is configured to serve as the PSC for the MSU HEV.

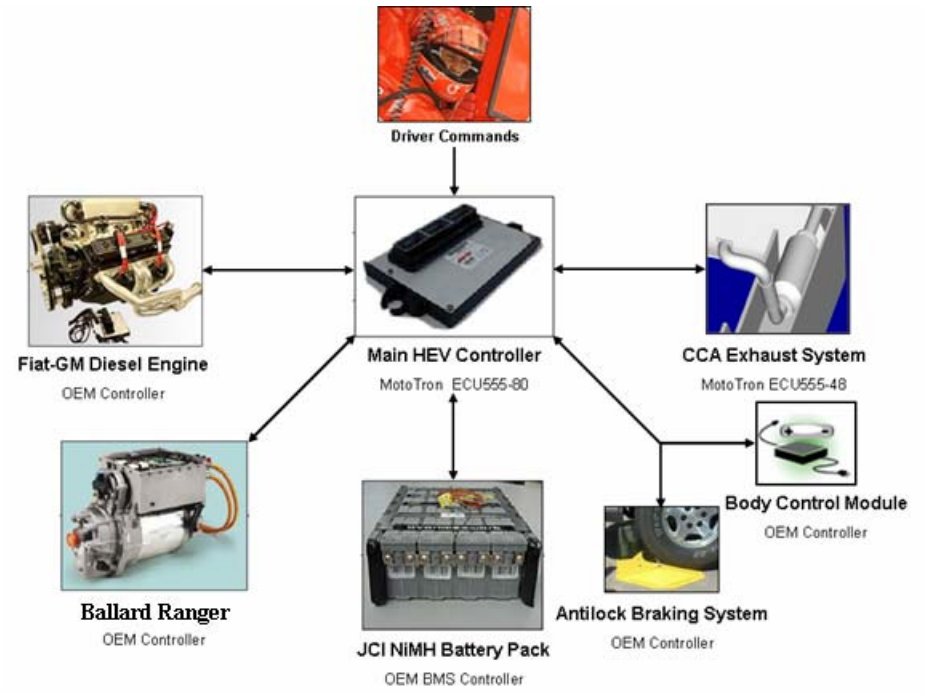

Figure 3.5: Hierarchy of Controllers in the MSU TTR parallel HEV

Based on the design objectives, an implemental control algorithm for the MSU HEV is developed. The strategy does not incorporate an engine idle-off feature and it does not include a pure electric launch mode. Engine idle-off refers to the approach of shutting down the engine when it is operating at or near the specified idling speed. Electric launch enables vehicle propulsion from standstill by means of the electric motor

alone. The strategy of not including engine idle-off and electric launch is pursued despite the relatively strong parallel hybrid configuration where peak power of the electric machine is approximately 38% of the cumulative engine and electric machine power and the electric machine is powerful enough to launch the vehicle by itself. This is primarily because engine idle-off and electric launch features tend to introduce a great degree of mechanical complexity in the powertrain and they will adversely affect vehicle driveability. It is realized that pure electric launch and instant restart of the diesel engine allow the engine to be shut down completely under inefficient operating conditions like low vehicle speeds and during engine idling. Without an engine idle-off state, the proposed full-time engine cruise strategy will not fully utilize the HEV capabilities of having dual power sources. But, the aforementioned approach will also ensure that all the possible advantages of engine downsizing and power blending are explored and the available regenerative braking capability is utilized to the maximum.

A notable factor in the control strategy is that the original bias between the driver accelerator pedal demand and engine torque output has been maintained, i.e. the driver accelerator request to the engine is interpreted as originally specified in the engine ECU. It is not altered or over-ridden in the HEV control strategy. For example, it may so happen that despite an accelerator pedal travel of 60%, a torque request corresponding to 75% accelerator pedal would force the engine to operate more efficiently. However, in the developed algorithm, the GM diesel engine ECU computes the torque request to the engine based on the original pedal request, without any interception. This is similar to providing a direct mechanical connection between the accelerator pedal and the engine

throttle. Thus, the engine load points cannot be manipulated and forced to operate in the most optimal region. This approach was also adopted in the Georgia Tech HEV [20].

The PSC must compute the torque request to the electric machine to ensure appropriate blending between the engine and the electric machine. The value of the torque request to the electric machine is obtained from continuously interpolating maps. These maps are based on the accelerator pedal position, the vehicle speed as a ratio of the maximum vehicle speed and the battery SOC. This is illustrated in Figure 3.6. The control methodology imparts adequate flexibility for manipulating only the electric drive system output while primarily concentrating on lowering overall fuel consumption and to some extent on engine NO_X emissions. It allows for *indirect* unloading of the engine thus lowering the instantaneous fuel flow rates to the engine [8, 26].

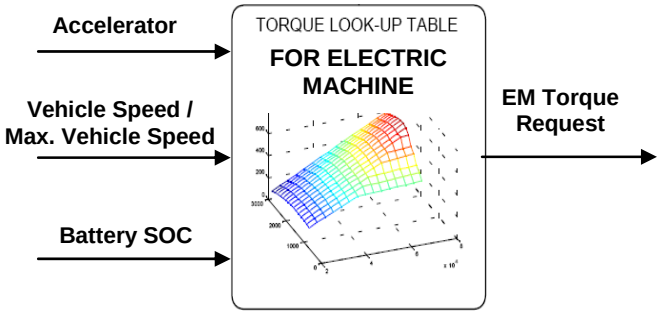

Figure 3.6: Illustration of Inputs for Electric Machine Torque Look-up

The primary modes of operation in the HEV control algorithm are engine-only, blending and braking. During the engine-only mode of operation, the vehicle is propelled by the engine alone while the HEV electrical subsystem provides no torque contribution. The electric machine is free-to-spin in this mode. This mode is activated when the clutch

is disengaged or the vehicle is stationary. This mode is also part of an emergency shut-down procedure for the electrical subsystem thereby allowing limp-home operation. Blending is the normal mode of operation of the MSU HEV and it includes logic for simultaneous operation of the engine and the electric machine based on different vehicle conditions. Operation during braking is described in the latter part of the discussion.

3.4 Description of the TTR Parallel HEV Control Algorithm

3.4.1 Propelling

Propelling, as defined in the control algorithm, occurs when the torque demand at the wheels is positive. The vehicle speed is varied by means of the accelerator pedal only and no brake pedal request is made by the driver. During normal operation of the HEV, blending between torques of the engine and the electric machine is activated when the clutch is engaged, a valid gear transmission ratio is detected and the vehicle is in motion. Blending includes logic for the following three distinct powertrain operating states.

1. Acceleration - when the vehicle velocity is increasing by at least a specific miles per hour per time instance.
2. Deceleration - when the vehicle velocity is decreasing by at least a specific miles per hour per time instance. This mode occurs when the driver releases the accelerator pedal, but the brake pedal is not depressed.
3. Cruising - when the road load and the vehicle velocity are constant. This mode encompasses steady states and ‘small’ accelerations and decelerations which do not necessarily require motor assist.

During acceleration, the electric machine provides boost torque to supplement the engine torque output. For all heavy to moderate accelerations, the electric machine contributes substantially to the powertain output to the wheels. The engine is indirectly unloaded while the electric machine supplements the high torque demands. Notably, for a WOT request, both the engine and the electric machine respond to the accelerator pedal position and provide the maximum available torques.

A unique provision has been incorporated in the control algorithm to avoid overcharging and deep discharging of the battery pack. In order to prevent excessive depletion of battery SOC during acceleration, positive torque is requested from the electric machine only when the SOC of the battery is greater than 30%. For SOC levels at or below 30%, zero torque is requested from the electric machine. Maximum positive torque is requested at and above an SOC of 90%. This upper SOC limit of 90% prevents battery overcharging during electric machine regeneration events, as will be seen in the electric machine torque maps for deceleration and cruising.

Table 3.2: Important Operating Parameters of the JCI NiMH Battery Pack [27]

BMS Parameter	Preferred Value
Maximum Discharge Current	200 A
Maximum Charge Current	150 A
Optimum SOC	30% to 75%
Optimum Operating Temperature	+15 °C to +45 °C

Table 3.2 lists some preferred battery management system (BMS) parameters of the 330 V NiMH battery pack. The recommended limits of SOC for efficient battery operation are between 30% and 75%. In the control algorithm, by choosing the lower and upper limits of 30% and 90%, respectively, it is also ensured that the battery operates within its optimal SOC limits as much as possible. The electric machine is allowed to operate at SOCs higher than the optimal upper limit of 75% (upto 90%) to prevent any compromise in HEV performance during heavy acceleration (WOT) events.

The electric machine torque contributions during acceleration were initially based on the plots used in the control strategy for the HEV designed by the Georgia Institute of Technology [20]. However, these plots compromised on HEV performance during WOT acceleration by requesting less-than-maximum values of motoring torque at low SOCs. This would in effect prevent consecutive, “true” WOT events thereby adversely affecting acceleration performance and reliability at low SOCs.

In the MSU control strategy, maximum motor assist is provided at WOT acceleration regardless of the SOC. For lower accelerator pedal requests, reduced motor torque is provided. At low SOCs, the driver must depress the accelerator pedal to a threshold level of pedal travel in order to request a positive torque output from the electric machine. With an increase in vehicle speeds, the accelerator pedal must be depressed further to receive a positive electric machine torque contribution at low SOCs. The electric machine torque at and above 90% battery SOC saturates to its maximum value at 50% of accelerator pedal travel for all vehicle speeds. However, for lower SOCs and faster vehicle speeds, the electric machine torque output reaches a steady value (less

than maximum torque) only at greater accelerator pedal travel. For an accelerator pedal travel beyond 90%, it is assumed that the driver intends to accelerate at WOT. The electric machine torque then gradually increases to its maximum torque output. Regardless of the accelerator pedal position, no torque is provided by the electric machine if the SOC is at or below 30%.

Sample maps for the electric machine torque output during acceleration at 25%, 50%, 75% and 100% of maximum vehicle speed for various battery SOCs are shown in Figures 3.7 to 3.10, respectively. The points of trend transitions in these maps have been intuitively calibrated by numerous simulations in Powertrain System Analysis Toolkit (PSAT) and on-road tests in order to ensure appropriate driver feel and to simultaneously meet the HEV performance requirements during acceleration.

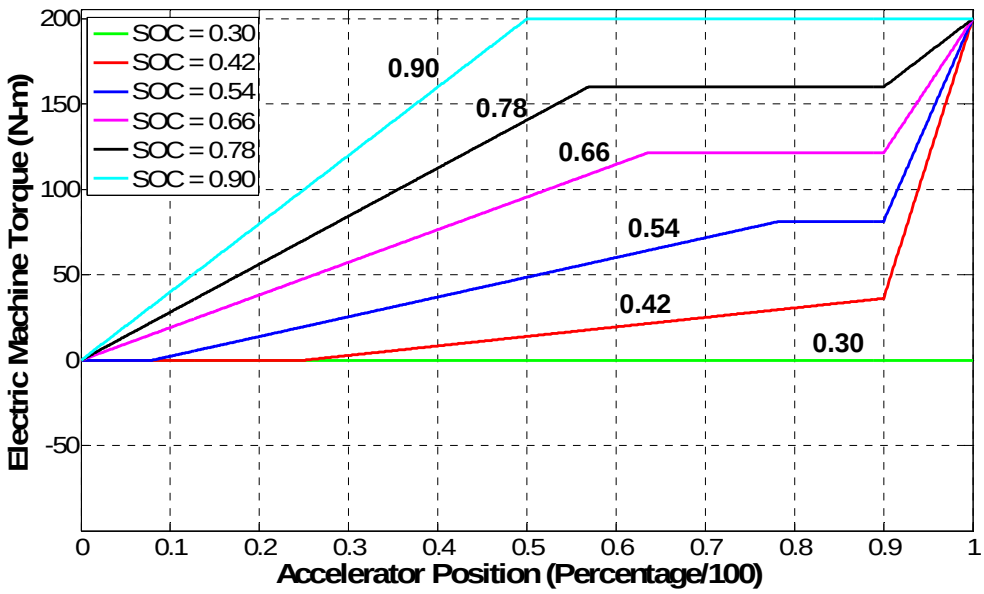

Figure 3.7: Electric Machine Torque Output vs. Accelerator Pedal Position for Various Battery SOCs at 25% of Maximum Vehicle Speed during Acceleration

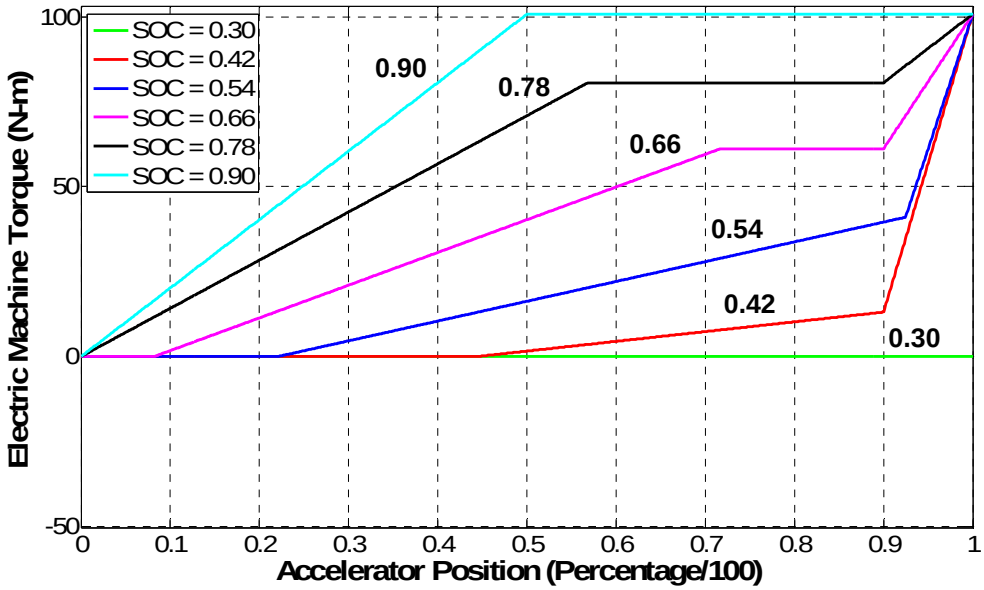

Figure 3.8: Electric Machine Torque Output vs. Accelerator Pedal Position for Various Battery SOCs at 50% of Maximum Vehicle Speed during Acceleration

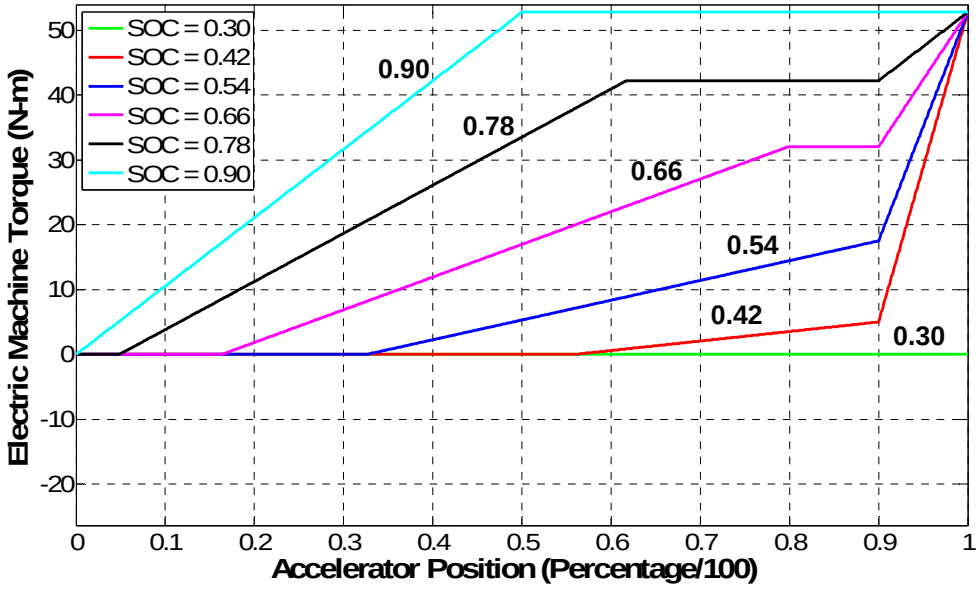

Figure 3.9: Electric Machine Torque Output vs. Accelerator Pedal Position for Various Battery SOCs at 75% of Maximum Vehicle Speed during Acceleration

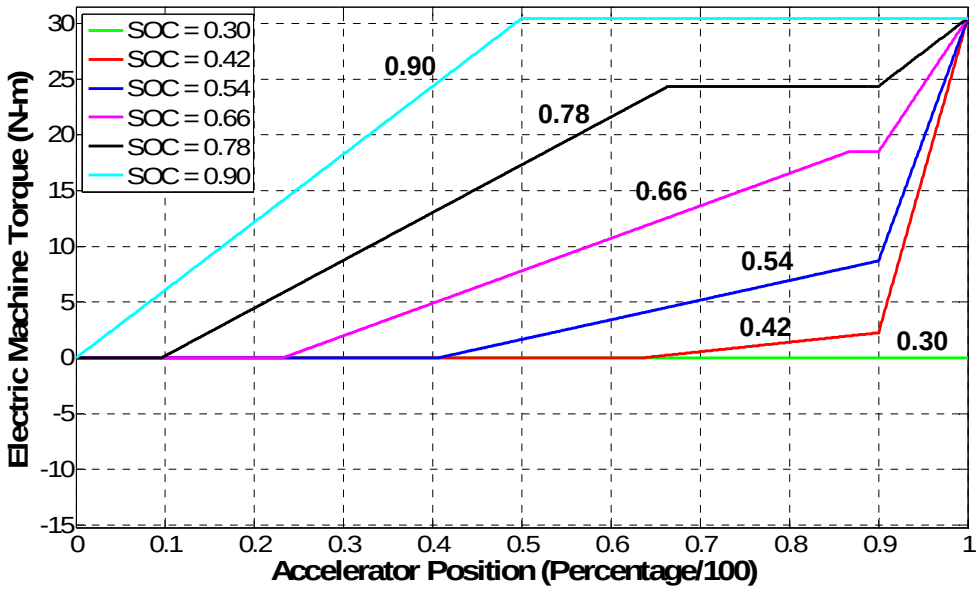

Figure 3.10: Electric Machine Torque Output vs. Accelerator Pedal Position for Various Battery SOCs at 100% of Maximum Vehicle Speed during Acceleration

Since the amount of electric machine assist is a function of driver torque demand, acceleration is a heavily charge-depleting mode of operation. The end of acceleration is marked by a drop in the driver torque demand thereby marking the end of electric machine assist. Cruising occurs when the vehicle has reached a steady state operating speed with only small variations in speed. During cruising, the most efficient operation is to fulfill the requested driver torque from the engine alone as in a conventional powertrain. The downsized engine is capable of operating near its WOT limit at lower engine speeds during cruising. An important point to note is that for a given engine output power level, minimum fuel is used as the speed of the engine is reduced [21].

In the MSU HEV, the electric machine is operated as a generator while cruising in order to restore some of the battery energy that may have been used in the accelerating

mode. This battery charging occurs at very low magnitudes of electric machine torque and this charging is important since it imparts a great deal of charge-sustaining capability to the parallel hybrid powertrain. The magnitudes of negative electric machine torques at lower SOCs are high and battery charging is gradually reduced to zero as the SOC approaches its maximum limit. Also, with an increase in vehicle speeds, the magnitude of charging is reduced in order to reduce the load on the engine and allow cruising at high speeds.

Sample maps for electric machine regeneration during cruising at 25%, 50%, 75% and 100% of maximum vehicle speed for various battery SOCs are shown in Figures 3.11 to 3.14, respectively. It is evident that the electric machine does not provide positive torque at any instance of vehicle cruising. Maximum regeneration always occurs at SOCs of 30% and less, while no regeneration is effected above 90% SOC. In fact at high SOCs, e.g. 0.78, regeneration occurs only at reasonably high vehicle speeds. PSAT simulations have been performed to estimate the effect of different levels of battery charging on the terminal SOC of the battery pack. These maps have been calibrated by on-road tests in order to ensure good driveability during cruising and for charge-sustaining operation during multiple drive cycles.

The deceleration mode occurs when the accelerator pedal is backed off (released) and no braking torque is requested. For that time instant, the electric machine regenerates at a much greater rate than during cruising. During cruising, the accelerator pedal request is fairly constant and the vehicle speed is steady. On the other hand, the action of releasing the accelerator pedal during deceleration is interpreted as an intention to reduce

the vehicle speed. It can also be gauged as a precursor to "coasting" without application of any accelerator or brake pedal requests or as an imminent sign of braking. Hence regeneration of the electric machine fulfills the intention of the driver to slow down the vehicle. Deceleration is a comparatively shorter and intermittent mode of operation and it imparts limited battery charging capability to the powertrain.

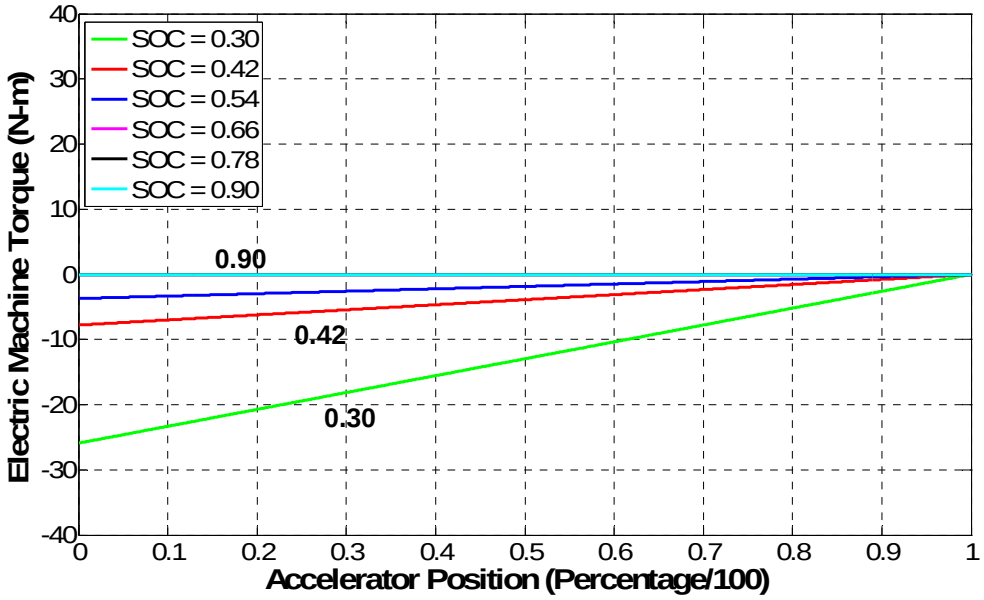

Figure 3.11: Electric Machine Torque Output vs. Accelerator Pedal Position for Various Battery SOCs at 25% of Maximum Vehicle Speed during Cruising

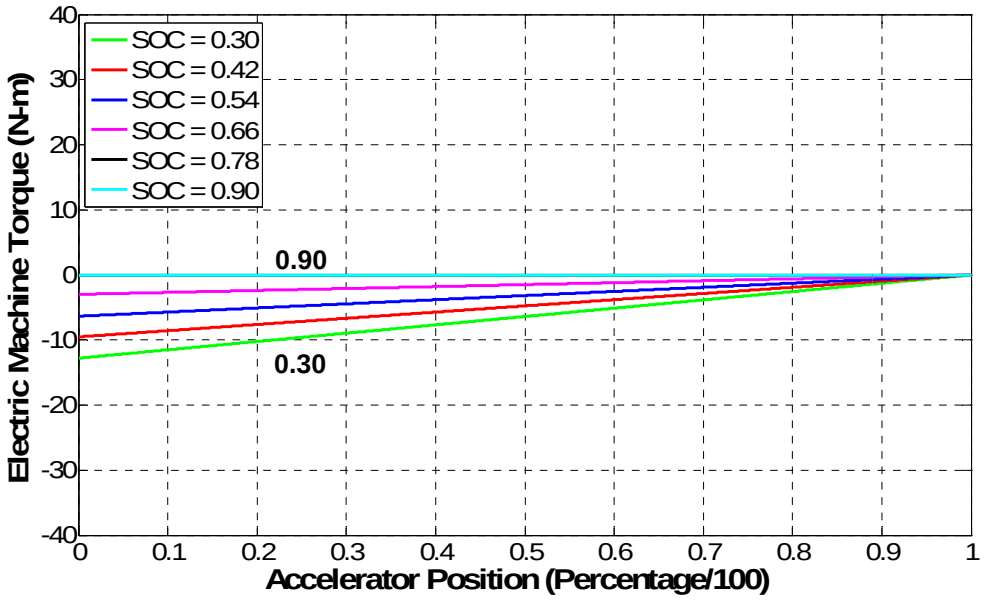

Figure 3.12: Electric Machine Torque Output vs. Accelerator Pedal Position for Various Battery SOCs at 50% of Maximum Vehicle Speed during Cruising

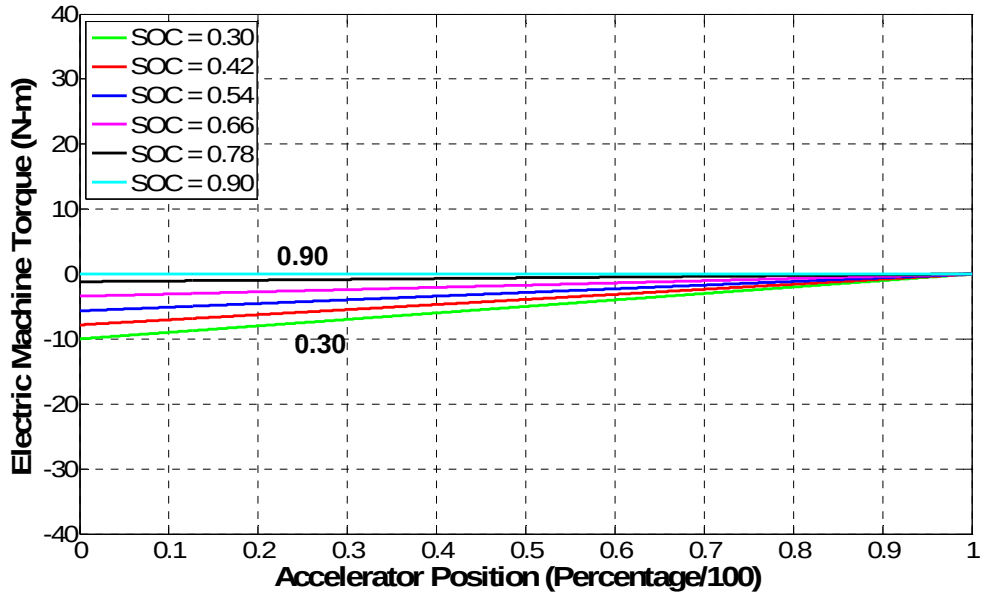

Figure 3.13: Electric Machine Torque Output vs. Accelerator Pedal Position for Various Battery SOCs at 75% of Maximum Vehicle Speed during Cruising

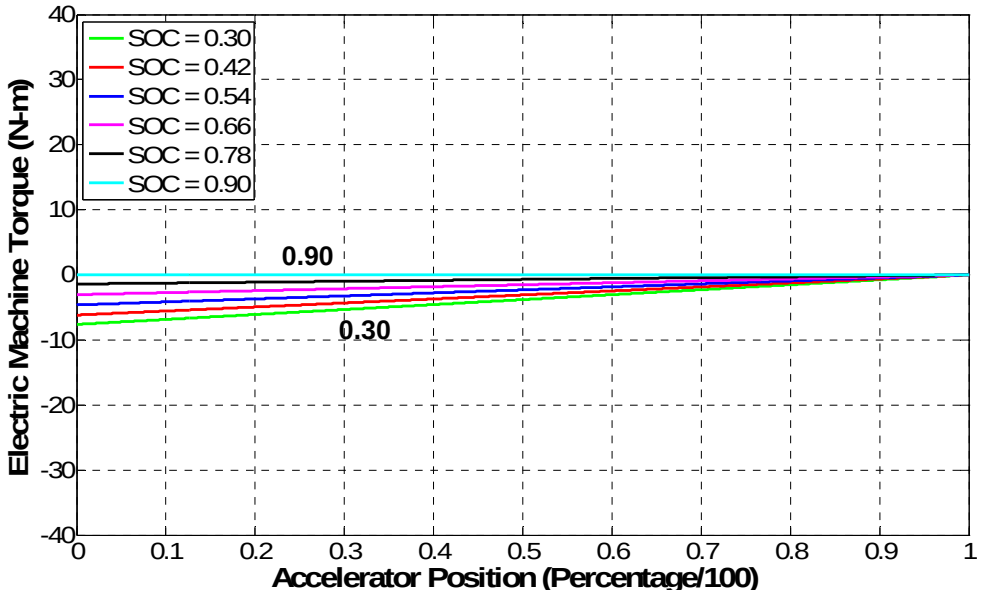

Figure 3.14: Electric Machine Torque Output vs. Accelerator Pedal Position for Various Battery SOCs at 100% of Maximum Vehicle Speed during Cruising

Sample maps for regeneration of the electric machine during vehicle deceleration at 25%, 50%, 75% and 100% of maximum vehicle speed for various battery SOCs are shown in Figure 3.15 to Figure 3.18, respectively. As seen, the trends during deceleration are identical to those during cruising, but of relatively higher magnitudes. The maps for deceleration have been calibrated through PSAT simulations and on-road tests in order to ensure a similar feel as experienced in a conventional vehicle.

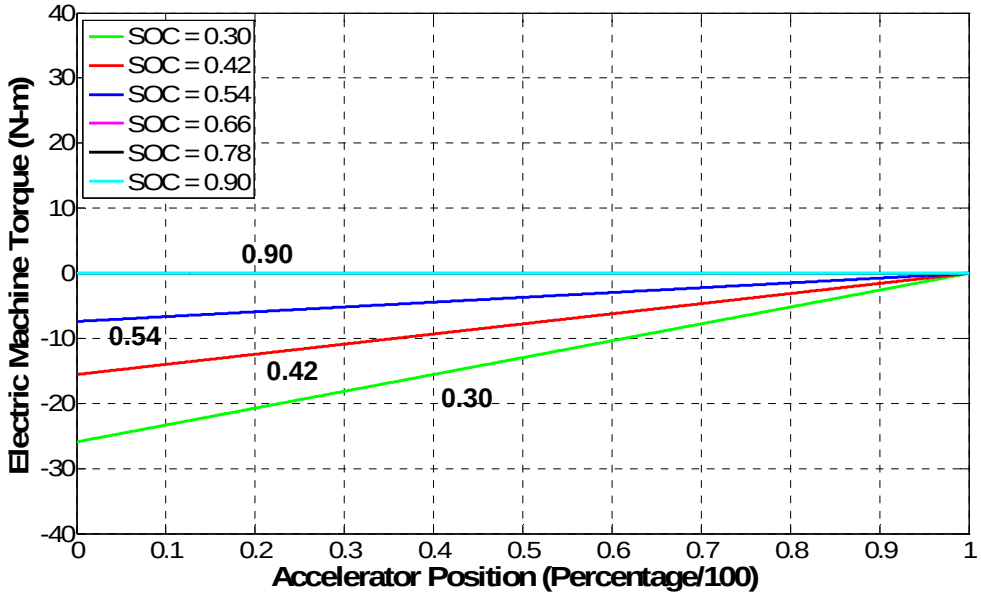

Figure 3.15: Electric Machine Torque Output vs. Accelerator Pedal Position for Various Battery SOCs at 25% of Maximum Vehicle Speed during Deceleration

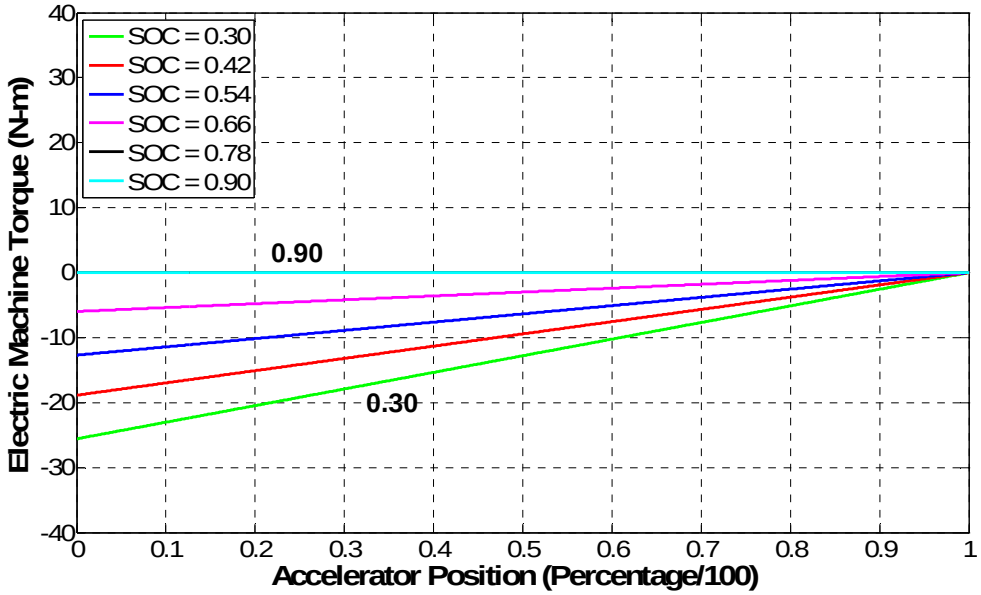

Figure 3.16: Electric Machine Torque Output vs. Accelerator Pedal Position for Various Battery SOCs at 50% of Maximum Vehicle Speed during Deceleration

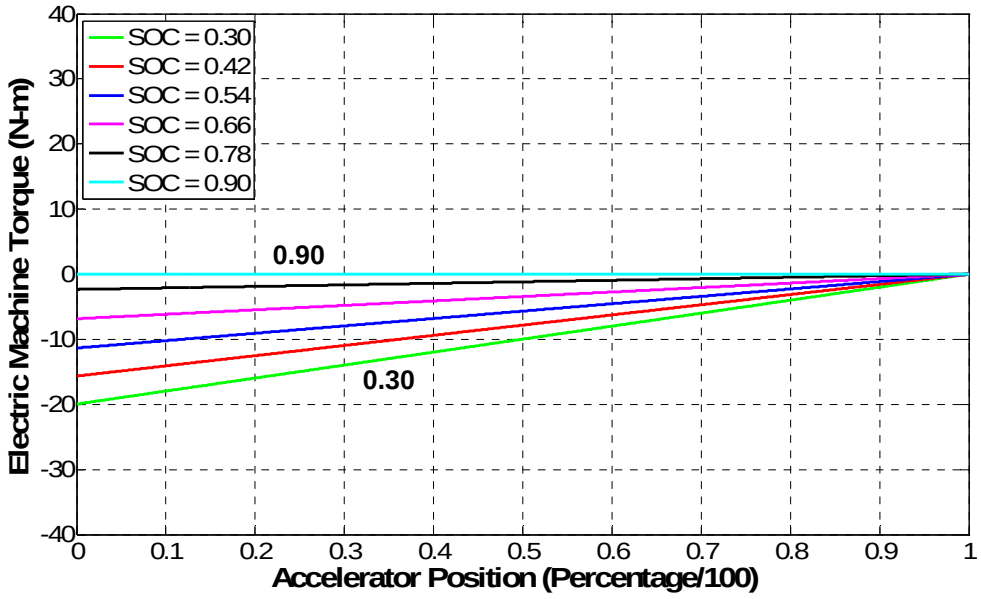

Figure 3.17: Electric Machine Torque Output vs. Accelerator Pedal Position for Various Battery SOCs at 75% of Maximum Vehicle Speed during Deceleration

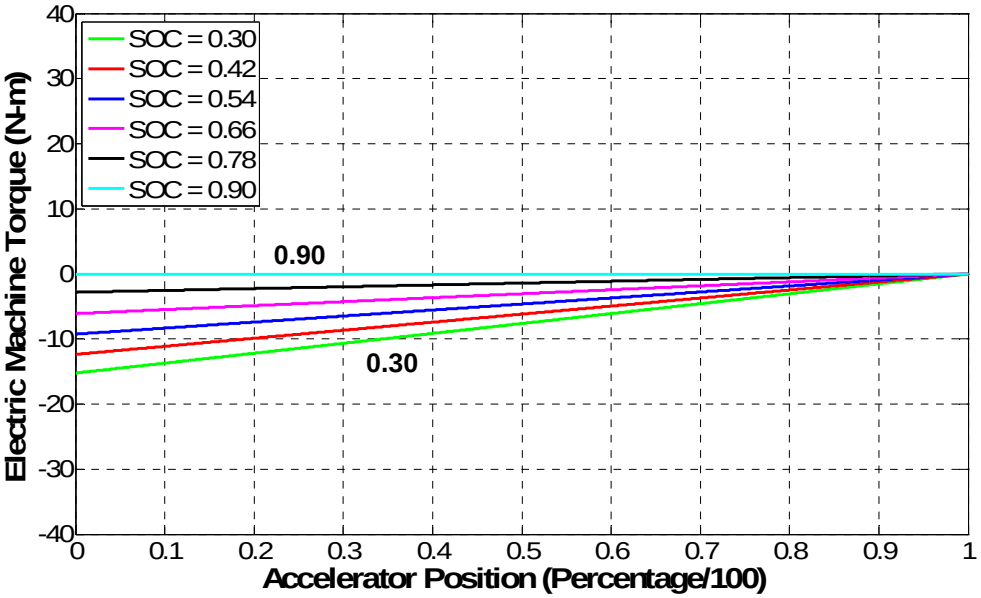

Figure 3.18: Electric Machine Torque Output vs. Accelerator Pedal Position for Various Battery SOCs at 100% of Maximum Vehicle Speed during Deceleration

Figure 3.19 illustrates the multidimensional look-up scheme between all the aforementioned propelling modes - acceleration, cruising and deceleration. The overall control algorithm is smoother and better coordinated due to the continuously interpolating nature of the electric machine torque outputs. Such an approach disregards the need for "hard" rules during mode transitions that sometimes tend to introduce unnecessary delays and discontinuities and make transitions from operating points on various maps easily noticeable while driving, thus adversely affecting the driveability.

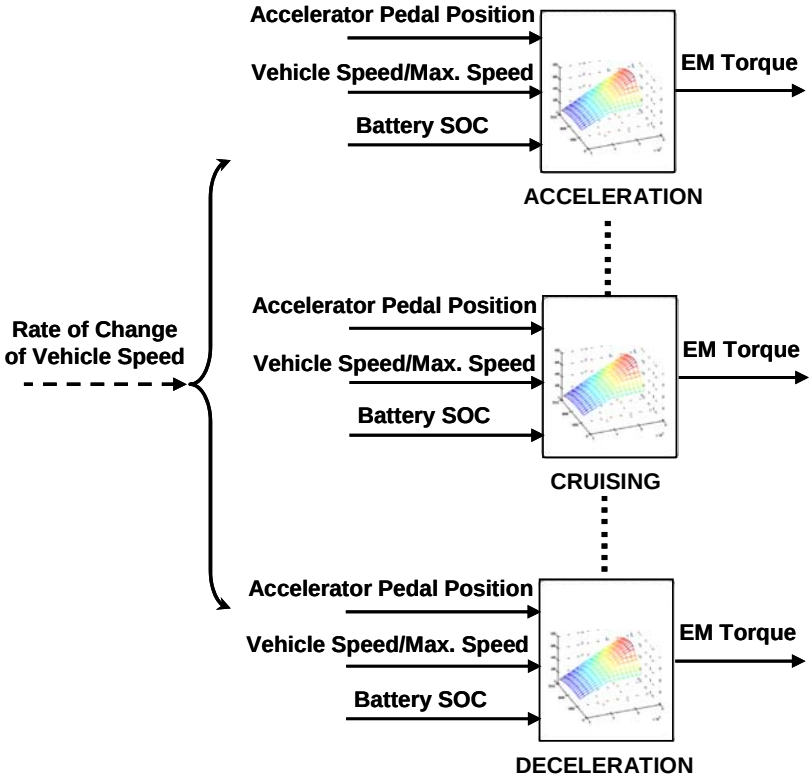

Figure 3.19: Illustration of Multi-dimensional Electric Machine Torque Look-up [8]

A decision as to the propelling mode of operation (acceleration, cruising or deceleration) is based on the rates of change of vehicle speed at a particular time. The threshold values of rates of change of vehicle speed for each of these modes have been intuitively calibrated by on-road tests. This is especially significant to maintain good driveability.

3.4.2 Braking

The overall performance of an HEV depends to a considerable extent on the type of braking adopted and the amount of regenerative energy recovered while doing so. Gain in fuel economy depends to a first order on the regeneration capabilities of the electric machine and then on the type of regenerative braking employed [7]. The regeneration power of the Ballard Ranger used in the MSU HEV is limited to 50% of its motoring capability. Hence it is imperative to maximize the amount of regeneration while braking.

The braking mode in the developed control strategy consists of coasting, split-parallel regenerative braking and friction braking. Coasting, as defined in this algorithm occurs when the driver does not command either the accelerator pedal or the brake pedal and the vehicle is free to roll. During coasting, electric machine regeneration is based on the vehicle speed and SOC of the battery pack. Figure 3.20 illustrates the look-up map used for this computation.

The initial trends for electric machine torques during coasting are plotted using the torque values during deceleration at exactly 0% accelerator pedal position for different SOCs and vehicle speeds. At higher values of SOC, virtually no battery charging is allowed. In order to ensure that vehicle is allowed to roll to a stop on account

of its own inertia and to maintain a similar feel as in a conventional vehicle, the trend lines are gradually converged to zero torque with a reduction in the vehicle speed.

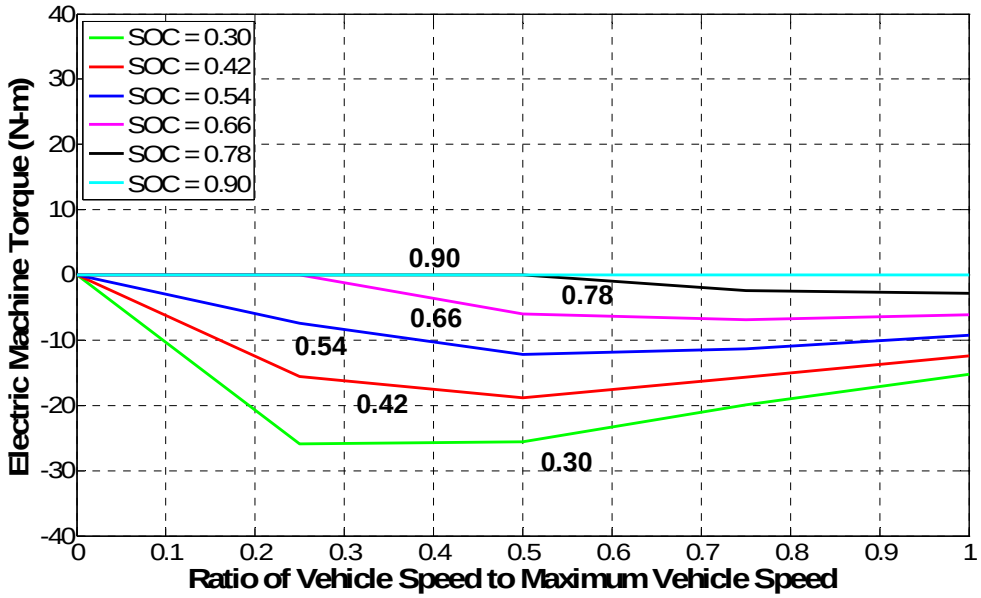

Figure 3.20: Electric Machine Torque Output vs. Ratio of Vehicle Speeds for Various Battery SOCs during Coasting

Figures 3.21 and 3.22 are simple depictions of series and parallel types of regenerative braking systems, respectively, that are prevalent in many present-day HEVs. Initial vehicle retardation due to engine compression braking is a common feature in many braking mechanisms. However, this is not a feature in the MSU HEV. Upon initial depression of the brake pedal in a series regenerative braking system (RBS), the electric machine regenerates and this regeneration has a pronounced effect on further depression of the brake pedal. The friction brakes engage only at a pre-defined point of brake pedal travel and blend with negative torque from the electric machine. In a parallel RBS, both

the friction brakes and the electric machine (generator) are instantaneously activated when the brake pedal is depressed. A control algorithm blends the friction brakes with regenerative torque to provide a smooth deceleration effect [7].

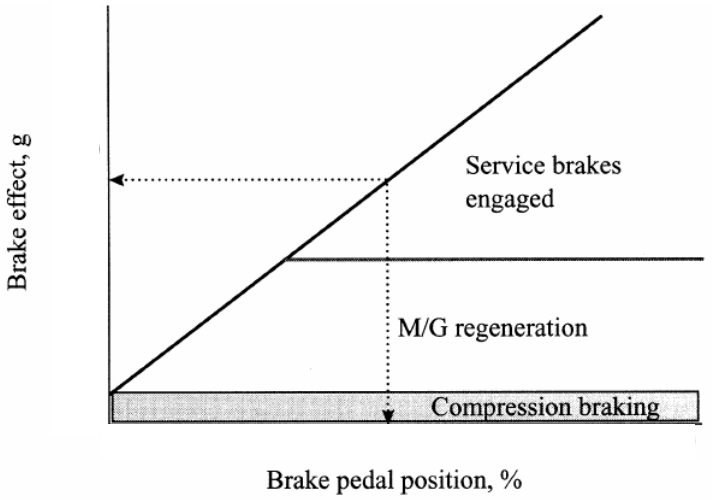

Figure 3.21: Series Regenerative Braking System [7]

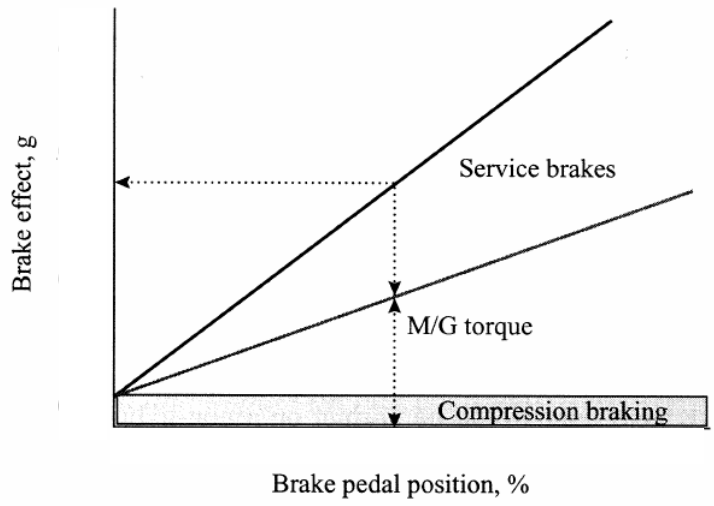

Figure 3.22: Parallel Regenerative Braking System [7]

Figures 3.21 and 3.22 do not account for complexities associated with braking systems in HEVs such as the proportioning of total braking effort between electric machine regeneration and friction brakes and the regeneration efficiencies of the electric machine.

In the braking strategy developed for the MSU HEV, a unique split-parallel regenerative braking system is employed. The underlying idea of split-parallel braking is to use the electric machine as much as possible for low-effort braking and engage the friction brakes only beyond a certain point of brake pedal travel. For a variable portion of the initial brake pedal travel, the friction brakes are not directly engaged. This variable portion of brake pedal travel depends on the intensity of depression of the brake pedal. During this period, only regenerative braking is employed based on an increasing percentage of negative torque request to the electric machine with respect to the brake pedal travel. The percentage of regenerative braking torque increases in magnitude until 32% of brake pedal travel and eventually saturates at its maximum value. This value of 32% pedal travel has been calibrated based on the mechanical modification to the master cylinder of the braking assembly, and has been explained later.

In the MSU HEV braking strategy, the minimum rotational speed of the electric machine for regeneration to occur has been set to 150 r/min (approximately 1 mi/h). Figure 3.23 is a graph of the spit-parallel regenerative braking system and separately shows the relationships between brake pedal travel and percentages of applied friction and regenerative braking torques [28, 29]. It is important to note that the trend for friction braking is merely a sample, and it varies based on the intensity of brake pedal depression.

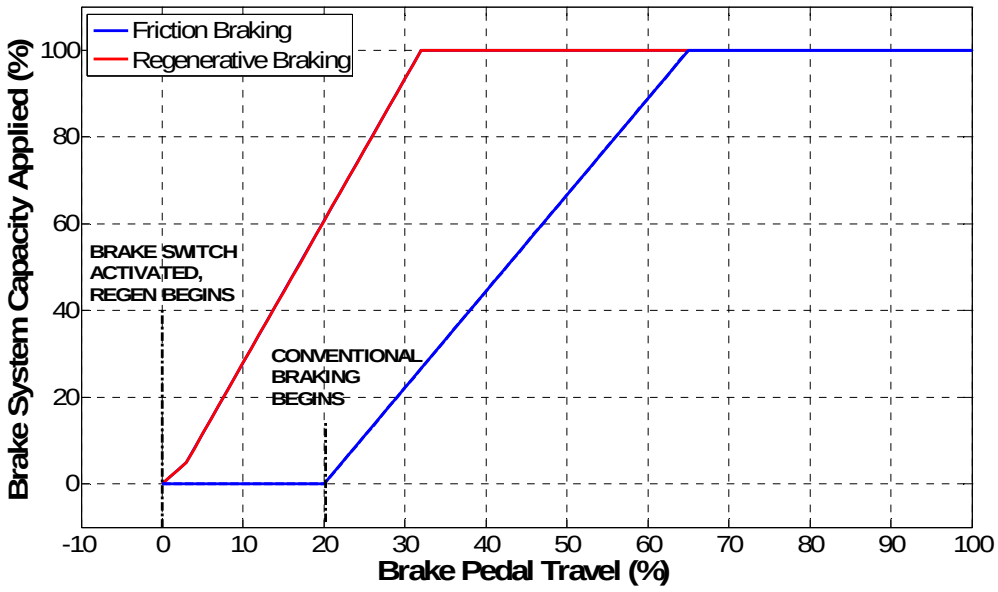

Figure 3.23: Split-parallel Regenerative Braking as Adapted in the MSU HEV [29]

In a conventional braking system, the brake pedal is mechanically connected to the master cylinder. The master cylinder is hydraulically linked to the braking devices at the wheels (disk or drum brakes) through brake lines. As the brake pedal is depressed, the pressure of the hydraulic fluid within the master cylinder increases, thereby increasingly actuating the braking devices at the wheels [28].

In the MSU HEV, the conventional master cylinder of the braking assembly has been mechanically modified and additional free-play at the top of the brake pedal travel is obtained. This is achieved by adding a small orifice (relief hole) to the internal bore of the brake master cylinder with relief to the brake fluid reservoir. A conventional master cylinder utilizes two pistons as a safety feature in the event brake fluid is lost at the front or rear brakes. The relief hole has been added to the front chamber and the diameter of

the hole is small enough to ensure that the original brake bias is maintained. The positioning of the hole is such that slow depression of the brake pedal allows the pressure in the master cylinder to drop momentarily, thus permitting a notable pedal travel before the conventional brakes are activated. Appropriate sizing of the hole ensures that brake fluid flow will be restricted during aggressive depression of the brake pedal. Rapid brake pedal action will cause the brake line pressure to rise during initial pedal travel and friction brakes will be activated instantaneously. In the event of slow brake pedal depression, the brake fluid will be relieved and regenerative braking will be predominant [28, 29]. Figure 3.24 illustrates the mechanical alteration made to the stock master cylinder.

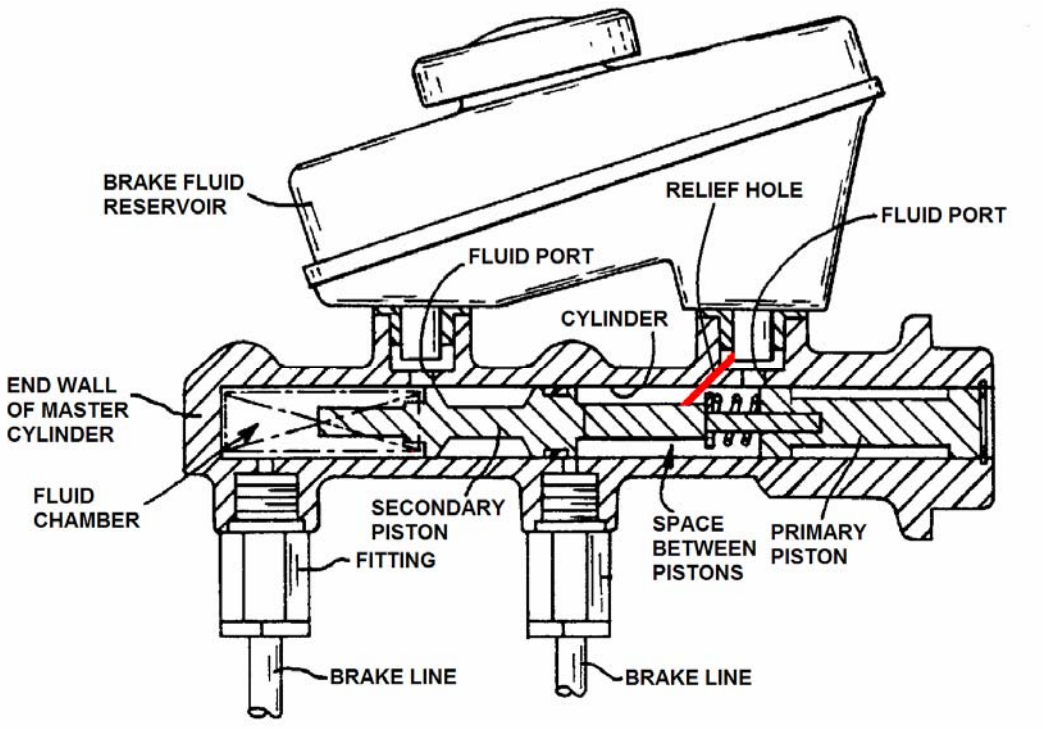

Figure 3.24: Conventional Master Cylinder and Mechanical Modification [28]

The biggest advantage of this simple mechanical modification is that it maintains the normal brake pedal feel during initial braking events, without compromising vehicle safety while allowing for electric machine regeneration.

3.5 Control Algorithm Development Platform

The Matlab™/Simulink™/Stateflow™ platform is used to develop the control algorithm for the HEV. A top-down, modular implementation approach has been adopted in compliance with Matlab Automotive Advisory Board (MAAB) guidelines for developing and refining the control algorithm in both simulated and real-time (RT) environments and to smoothly transition between them. Native Simulink block diagrams can represent signal processing very well and have been used for modeling complex math models of the plant as advised in the MAAB guidelines. The biggest advantage of using Simulink to devise the control strategy is the ability to transfer the model directly onto the controller by auto code generation without having to write production code by hand.

Stateflow is primarily employed to specify dedicated control logic in the controller. The control algorithm has been designed as a finite state machine of different modes of operation (blending, braking and engine-only operation) described earlier. This ensures that the algorithm is restricted to run in only one state at any instant of time and each state can be tested and debugged separately. The power of Stateflow lies in its abilities as a visual programming tool to easily depict complex and cascading logic statements for decision-making, execute the developed logic by animating the logic diagram and finally debug them at will by placing breakpoints at important junctures.

CHAPTER 4

ANALYSES AND VALIDATION OF SIMULATION AND ON-ROAD TEST RESULTS

4.1 Vehicle Simulator - PSAT™

The control algorithm developed for the MSU HEV configuration has been analyzed using the Powertrain System Analysis Toolkit (PSAT), a command-based, forward-facing vehicle simulator developed at Argonne National Laboratory. PSAT is based upon the Matlab/Simulink/Stateflow environment and possesses real-world simulation attributes. The forward-facing approach refers to simulations that iteratively modify individual component control commands to various vehicle subsystems while attempting to minimize the error between driver demand and actual vehicular system response. The command-based, real-world feel to forward-facing simulation is imparted by the inclusion of a driver model which, in an attempt to follow a pre-defined speed cycle, considers the present speed and desired speed to develop appropriate commands for propelling, braking and gear shifting. The throttle and brake commands are translated to torque requests from the various power sources in the powertrain [30].

Forward-facing models deal in quantities that can be measured in the actual drivetrain such as control signals and 'true' torque values and hence are desirable for detailed control simulation and vehicle controller hardware development. Flexibility to use dynamic models and true computation of maximum-effort accelerations (WOT

events) renders use of the forward-facing approach in RT control strategy development. The forward-facing approach of vehicle simulation is computationally more intensive than backward-facing simulation. This is because higher-order integration schemes using relatively small time steps are necessary to provide stable and accurate simulation results. Hence the simulation can be time-consuming [30]. Among the other highlighting characteristics of PSAT that are useful to the HEV development cycle are flexibility to exchange control strategies, easily exchangeable component models and capability to run batch mode operation. On the other hand, PSAT does not support component calibration or study of driveability [31].

Unlike the forward-facing approach, backward-facing simulation assumes that the vehicle has met the driver demand and then computes individual component performance. ADVISOR™ – a vehicle simulator developed by National Renewable Energy Laboratory (NREL) uses a hybrid backward/forward approach that is closely related to the strictly backward-facing approach. The biggest drawback of this approach vis-à-vis real-life component interactions is the lack of a driver behavioral model and the absence of control signals like throttle and brake position thus hindering dynamic system simulation and control system development [30].

4.2 Drive Cycles

The performance of the developed control algorithm was tested by running the MSU HEV on a four-wheel chassis dynamometer over four standard drive cycles for light duty vehicles in the United States at varying values of initial SOC (β). The different values of initial SOCs considered were 45%, ($\beta_1 = 0.45$), 65% ($\beta_2 = 0.65$) and 85% ($\beta_3 =$

0.85). The drive cycles were chosen such that they represented diverse, real-world and regular driving schemes. The HEV was analyzed for the Federal Test Procedure – 72 (FTP – 72), Highway Fuel Economy Test (HWFET), Federal Test Procedure – 75 (FTP – 75) and US06 Supplemental Federal Test Procedure (SFTP) [32].

4.2.1 Federal Test Procedure – 72 (UDDS)

Commonly known as the Urban Dynamometer Driving Schedule (UDDS) or the LA-4 cycle, this drive cycle simulates an urban route of about 7.5 miles with frequent stops. The maximum speed is 56.7 mi/h and the average speed is 19.6 mi/h. The entire cycle of 1369 seconds consists of two phases – Phase I (505 seconds) and Phase II (864 seconds). Phase I is 3.59 miles at an average speed of 25.6 mi/h. This is more aggressive than phase II which has an average speed of 16.3 mi/h. The two phases are separated by stopping the engine for 10 minutes [33].

4.2.2 Highway Fuel Economy Test (HWFET)

The HWFET is a driving schedule for determining the fuel economy of light-duty vehicles when driving on the highway. The cycle lasts for 765 seconds and covers a total distance of 10.26 miles at an average speed of 48.3 mi/h. This cycle was developed by the U.S. Environmental Protection Agency (EPA) [33].

4.2.3 Federal Test Procedure – 75 (FTP – 75)

The FTP-75 has been primarily used for emissions certification of light duty vehicles in the U.S. It is essentially derived from the FTP-72 (UDDS) by adding an additional phase of 505 seconds that is identical to the first 505 seconds of the FTP-72.

This cycle traverses approximately 11.04 miles for a duration of 1874 seconds at an average speed of 21.2 mi/h [33].

4.2.4 US06 Supplemental Federal Test Procedure (US06 SFTP)

Despite the transient nature of the FTP-75, the average speed of the cycle is quite low. The US06 drive cycle tries to address the shortcomings of the FTP-75 drive cycle in the representation of aggressive, high speed and/or high acceleration driving behavior and rapid speed fluctuations. Both the average speed of 48.4 mi/h and the top speed of 80.3 mi/h are much higher than the corresponding values in the FTP-75 (and also the UDDS) indicating its more aggressive nature. The cycle lasts for 596 seconds and traverses a 8.01 mile route [33].

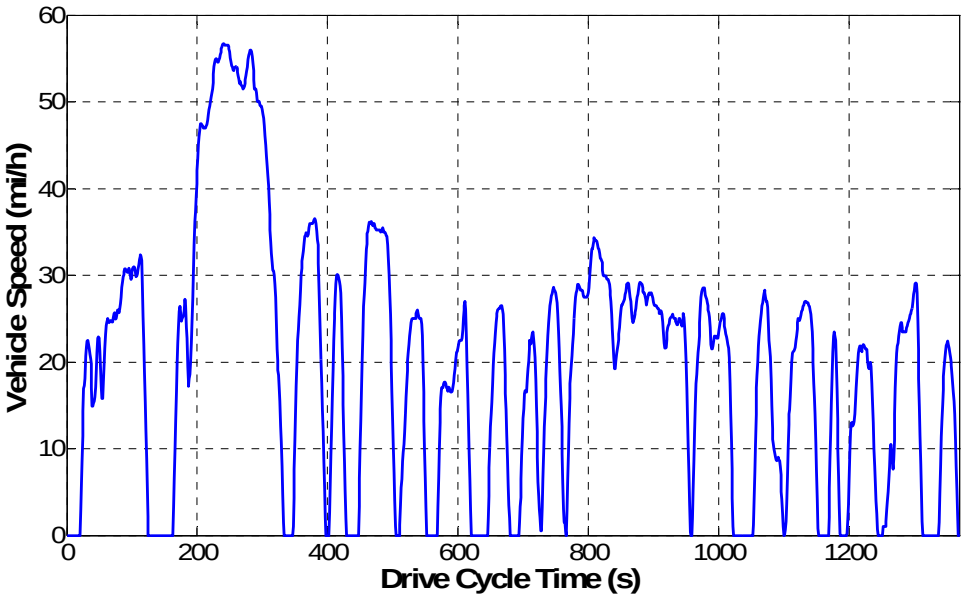

Figure 4.1: Speed Profile for the Federal Test Procedure – 72 (UDDS)

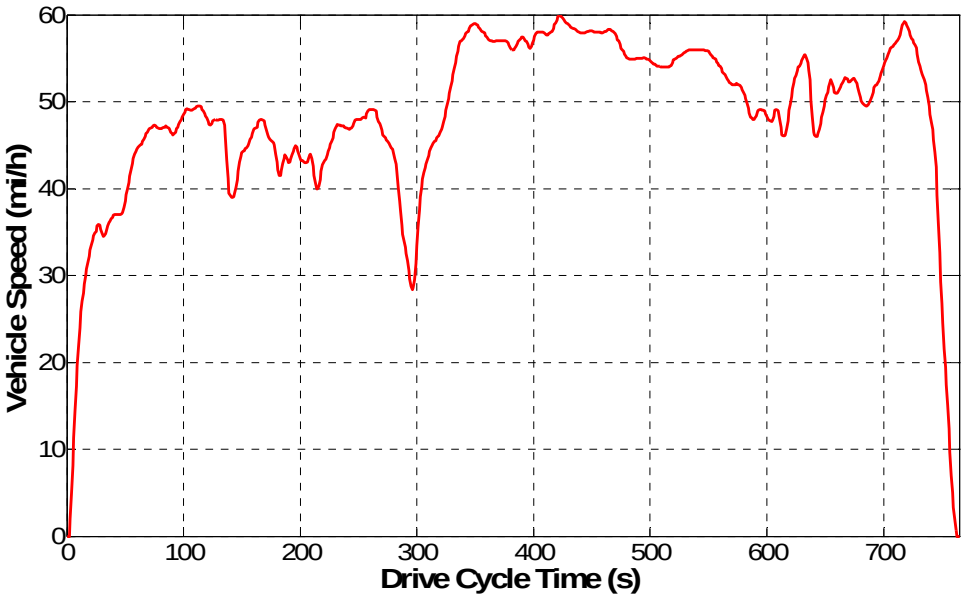

Figure 4.2: Speed Profile for the Highway Fuel Economy Test (HWFET)

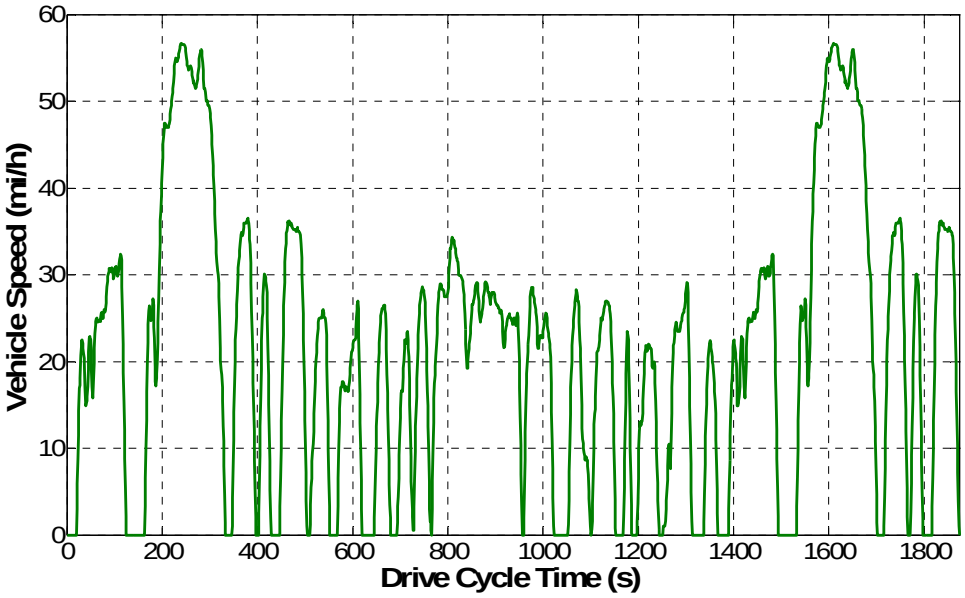

Figure 4.3: Speed Profile for the Federal Test Procedure – 75 (FTP-75)

Figure 4.4: Speed Profile for the US06 Supplemental Federal Test Procedure (US06)

The US06 SFTP along with SC03 SFTP, which addresses the use of air-conditioning in light duty vehicles, have been used for mandatory testing of vehicle models beginning model year 2000. It is also interesting to note that the US06 involves a significant portion of high-speed highway driving. The average speed of the US06 is comparable to that of the HWFET [33].

4.3 PSAT Simulation Results and On-Road/Chassis Dynamometer Test Results

4.3.1 IVM to 60 mi/h and 50 to 70 mi/h Acceleration Tests

Table 4.1 lists the comparison of acceleration times for initial vehicle movement (IVM) to 60 mi/h and 50 to 70 mi/h.

Table 4.1: PSAT Simulation and On-Road Test Results for the IVM to 60 mi/h and 50 to 70 mi/h Acceleration Events

Category Description	PSAT Simulation	On-Road Results
IVM to 60 mi/h Acceleration	8.30 s	8.17 s
50 to 70 mi/h Acceleration	5.20 s	4.68 s

The following section analyzes the performance of the MSU HEV during the IVM to 60 mi/h and 50 to 70 mi/h on-road acceleration tests. Figure 4.5 shows the variation of vehicle speed and battery SOC during the IVM to 60 mi/h on-road acceleration event. Initial transients in engine torque and slippage of the front wheels lead to a sudden increase in vehicle speed from standstill for a very short period. The vehicle speed then increases steadily during the rest of the acceleration event. As anticipated, the battery SOC reduces since the electric machine operates as a motor to provide torque in addition to the engine torque for acceleration. The battery SOC is observed to decrease in steps since the BMS is capable of computing the SOC in integer values only. Figure 4.6 shows that the electric machine torque peaks during the initial launch from standstill and later reduces gradually. The engine operates near WOT at most times except during initial operation and during gear shifting. During shifting, the clutch is disengaged and the engine torque reduces considerably. The engine torque increases gradually only when the clutch is engaged. This is also evident from Figure 4.7 that shows the scatter of engine operating points during the IVM to 60 mi/h acceleration.

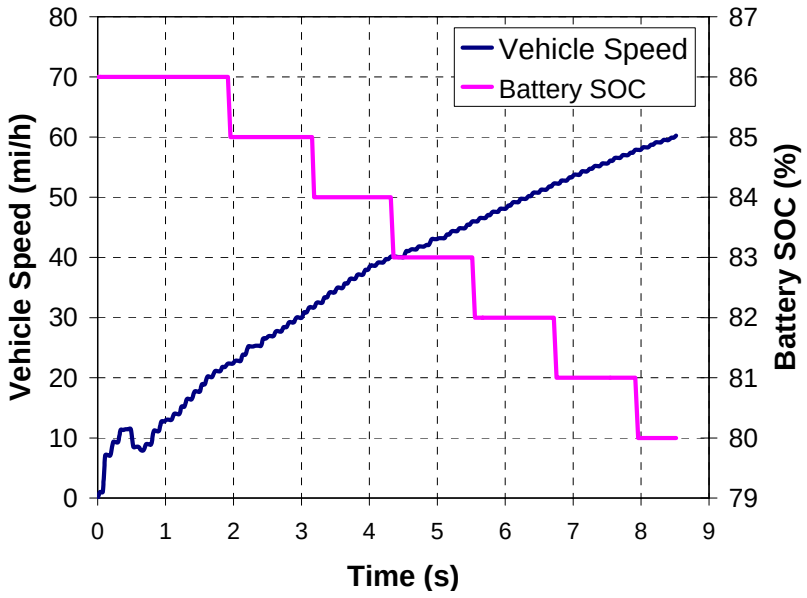

Figure 4.5: Variation of Vehicle Speed and Battery SOC during IVM to 60 mi/h Acceleration (On-Road Test Results)

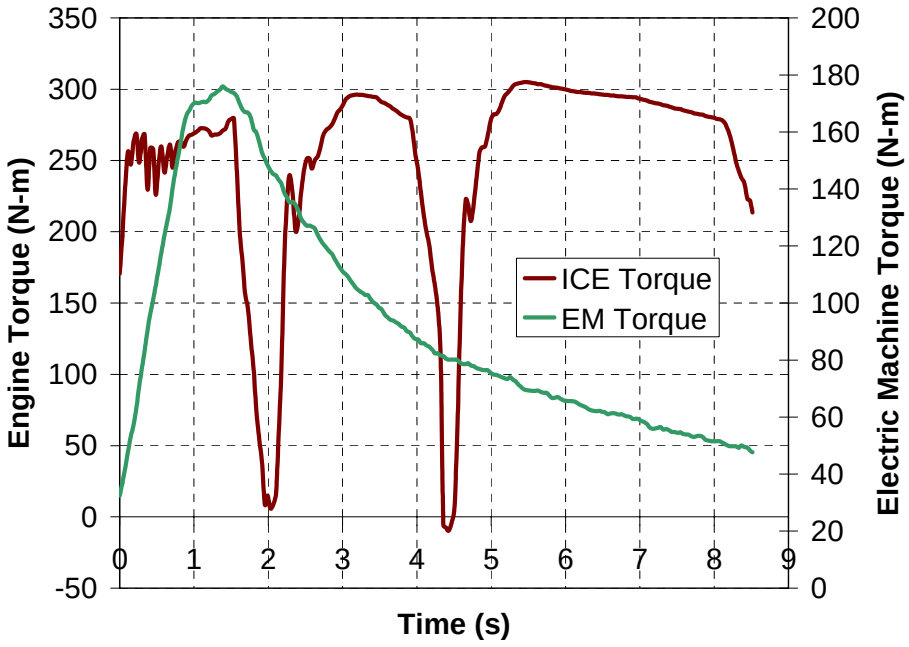

Figure 4.6: Measured Engine and Electric Machine Torques during IVM to 60 mi/h Acceleration (On-Road Test Results)

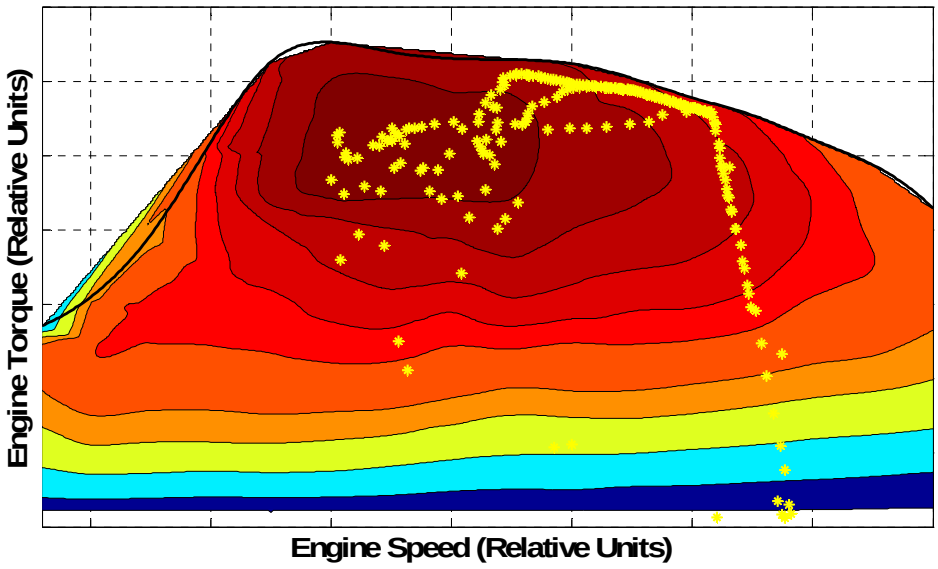

Figure 4.7: Engine Operating Points during IVM to 60 mi/h Acceleration (On-Road Test Results)

Figure 4.8 shows the vehicle speed that undergoes a steady increase during the 50 to 70 mi/h on-road acceleration event. The battery SOC gradually reduces since the electric machine operates as a motor to provide additional torque for acceleration. The engine torque, as seen in Figures 4.9 and 4.10, is always concentrated near the WOT region. It does not drop to low values at any instant since this acceleration does not involve gear shifting. The electric machine provides a near-constant torque.

The engine operates at WOT during a substantial portion of both the acceleration events. The electric machine thus plays an important role in ensuring that the HEV performance requirements during acceleration are met despite the downsized engine. Improvements of 3.89% and 25.71% over the stock vehicle IVM to 60 mi/h and 50 to 70 mi/h acceleration times respectively, are obtained.

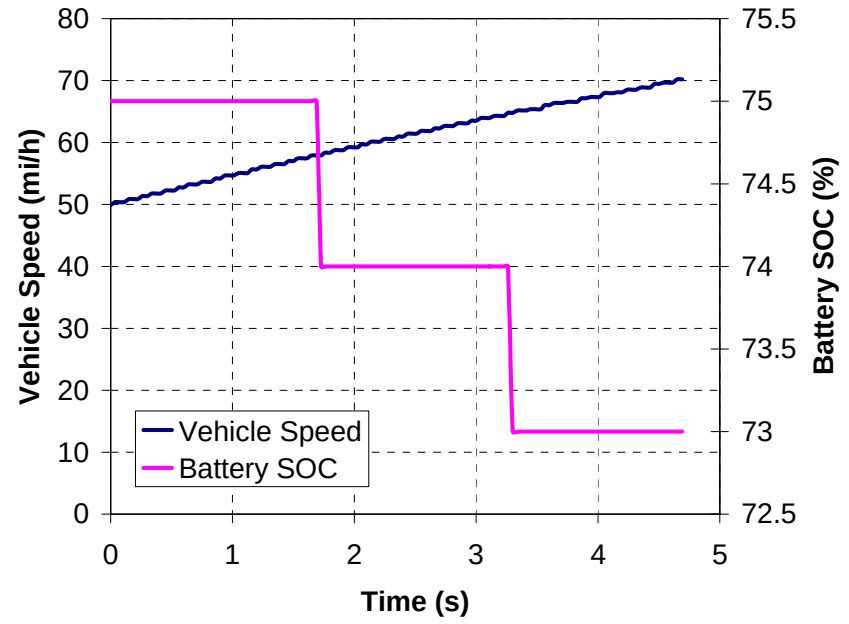

Figure 4.8: Variation of Vehicle Speed and Battery SOC during 50 to 70 mi/h Acceleration (On-Road Test Results)

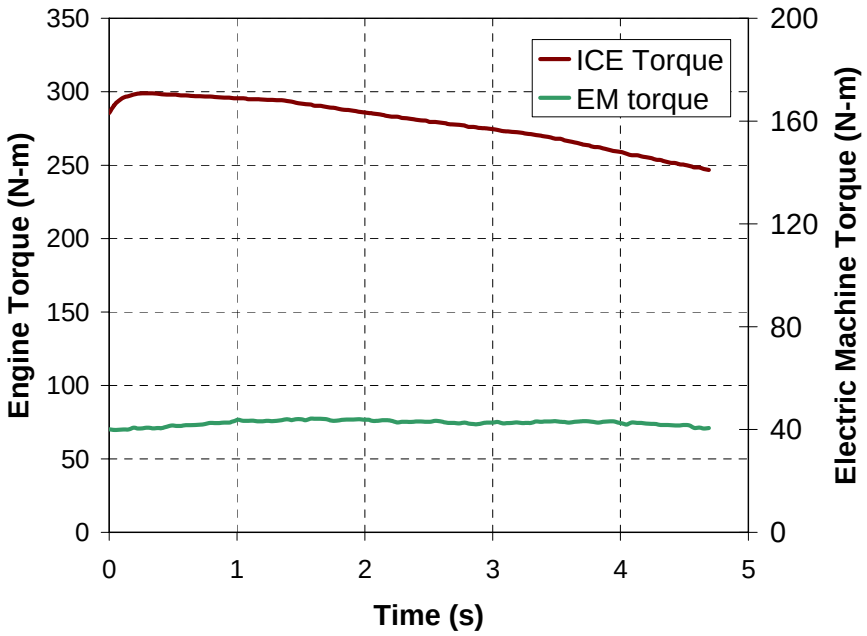

Figure 4.9: Measured Engine and Electric Machine Torques during 50 to 70 mi/h Acceleration (On-Road Test Results)

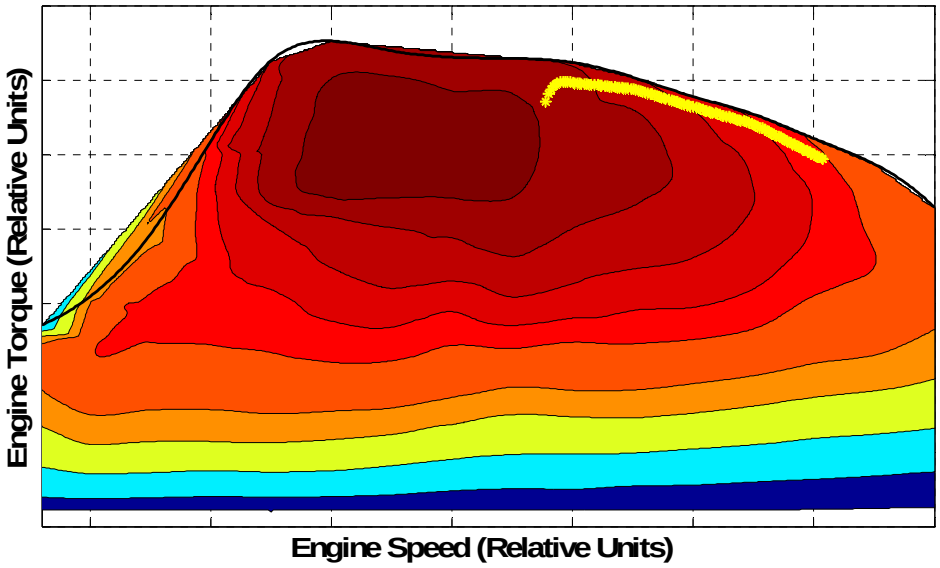

Figure 4.10: Engine Operating Points during 50 to 70 mi/h Acceleration (On-Road Results)

4.3.2 Federal Test Procedure – 72 (UDDS)

Table 4.2 includes RT data from the chassis dynamometer tests for the UDDS drive cycle in diesel engine-only and hybrid configurations at initial SOCs of 45%, (β_1 = 0.45), 65% (β_2 = 0.65) and 85% (β_3 = 0.85). PSAT predictions for several drive cycles including the UDDS at the same initial SOCs of β_1, β_2, and β_3 have been presented in Appendix A. Predictions of the fuel economy obtained from PSAT simulations do not match closely with the dynamometer test results. This is primarily because of the differences in the computed fuel consumption and the final SOCs at the end of drive cycle. It is observed that PSAT calculations tend to overestimate both the motoring and regenerative contributions of the electric machine. Increased electric machine torque contribution during propelling leads to lower engine fuel consumption while more

regeneration than actual causes higher terminal SOCs of the battery pack. These factors have a cumulative effect on raising the predictions of fuel economy. Also, PSAT does not account for RT driving considerations such as atmospheric temperature, driver behavior, etc. all of which have a considerable effect on the performance.

PSAT has been used to analyze trends and gauge the effects of changes to the control strategy on the HEV performance. The above observations are also applicable to all the other the drive cycles considered in this thesis.

Table 4.2: Chassis Dynamometer Test Results for the UDDS Drive Cycle

Description	UDDS – Diesel Only	UDDS (β1)	UDDS (β2)	UDDS (β3)
Initial SOC	-	0.45	0.65	0.85
Final SOC	-	0.61	0.64	0.67
Fuel Consumed (gal)	0.30	0.31	0.28	0.25
B20 Fuel Economy (mi/gal)	25.11	24.40	26.45	29.20
SOC Corrected B20 Fuel Economy (mi/gal)	25.11	28.51	26.45	24.69
Gasoline Equivalent (mi/gal)	21.06	20.47	22.18	24.48
SOC Corrected Gasoline Equivalent (mi/gal)	21.06	23.91	22.18	20.71

The need for SOC correction and the method of calculations have been described in Appendix B. The fuel economy of the stock vehicle for the UDDS as per its technical specifications is 19 mi/gal [23]. From Table 4.2, it is seen that the HEV fuel consumption decreases with an increase in the initial SOC of the battery. Figures 4.11 to 4.14 show

that the scatter of engine operating points during UDDS is generally concentrated in areas of low engine power requirement. With an increase in the initial SOC of the battery, a noticeable shift in the scatter of engine operating points to regions of low fuel flow rate is observed. The electric machine helps to unload the engine of the few relatively high torque operating points, depending on the battery SOC.

At a high initial SOC of 85%, the electric machine contribution is significant and it reduces the load on the engine thus reducing fuel consumption but simultaneously depleting the battery SOC. The performance of the HEV at an initial SOC of 65% is better than that of diesel engine-only configuration and the SOC is maintained. However when β equals 45%, the electric machine has limited capabilities to unload the engine. In fact, the engine performs additional work to charge the battery and hence causes greater fuel consumption. In this case, the control strategy performs a good function of raising the battery SOC by the end of the cycle, at the sacrifice of some fuel consumption.

Table 4.3 lists the percentage improvements obtained due to powertrain hybridization over the stock gasoline and diesel engine-only vehicle configurations for the UDDS drive cycle. Negative percentage values indicate a loss of fuel economy. In order to compare the MSU HEV (which uses B20 biodiesel) with the stock vehicle (which is gasoline operated), the B20 fuel economy has been converted to its gasoline equivalent (GE) value. It can be seen that the percentage gains in fuel economy (including SOC corrected fuel economy) over the diesel engine-only configuration during the UDDS drive cycle are not as significant as the gains over the stock gasoline vehicle.

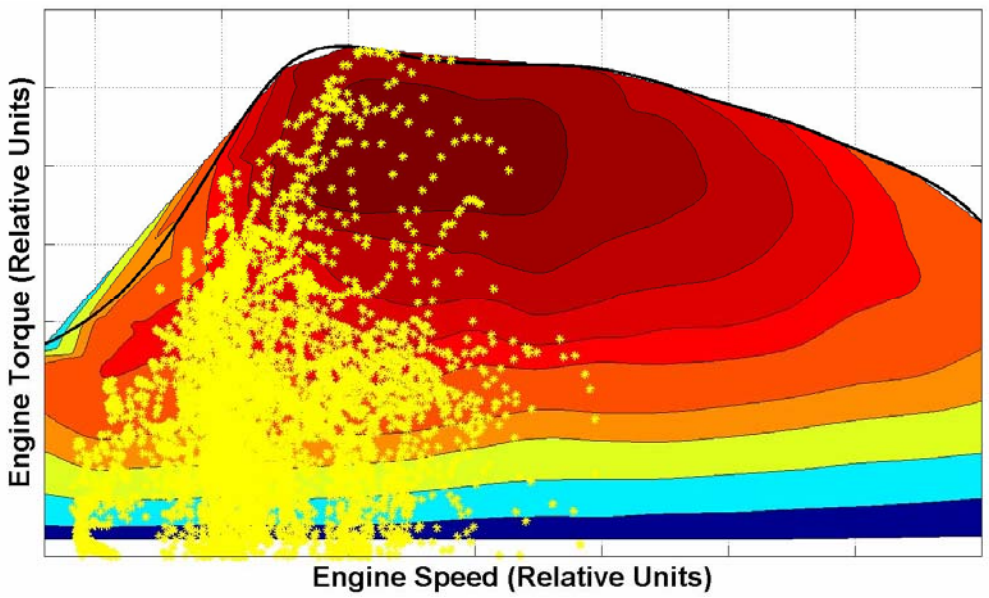

Figure 4.11: Engine Operating Points for the UDDS Drive Cycle in Diesel Engine-only mode (Chassis Dynamometer Test Results)

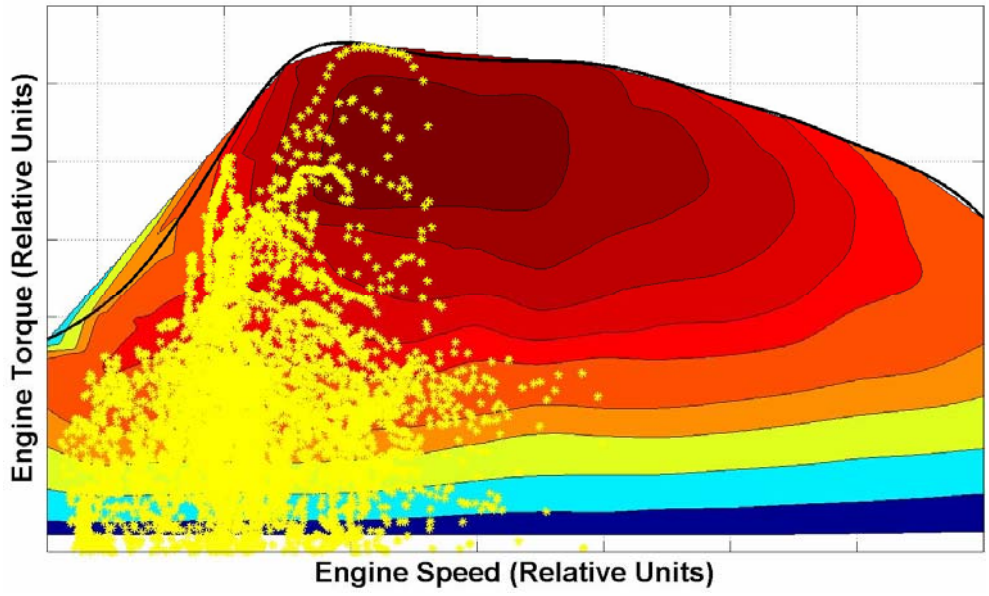

Figure 4.12: Engine Operating Points for the UDDS Drive Cycle in Hybrid Mode at $\beta = 0.45$ (Chassis Dynamometer Test Results)

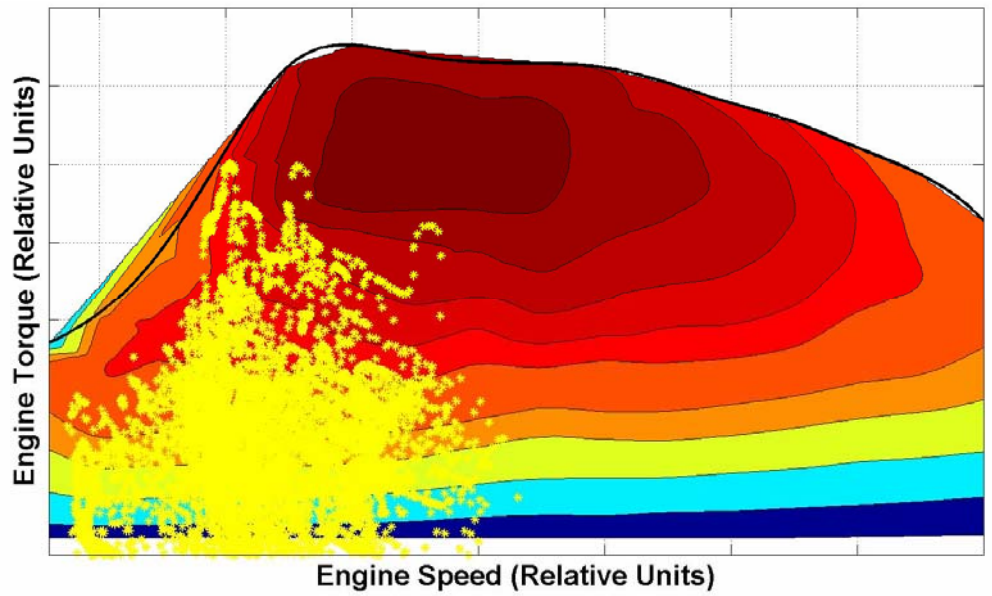

Figure 4.13: Engine Operating Points for the UDDS Drive Cycle in Hybrid Mode at $\beta = 0.65$ (Chassis Dynamometer Test Results)

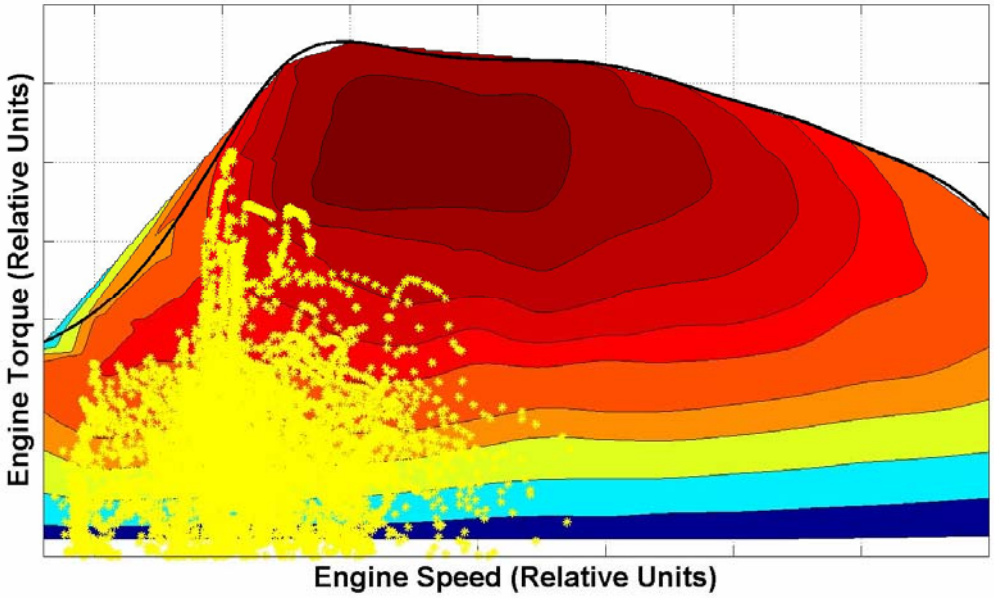

Figure 4.14: Engine Operating Points for the UDDS Drive Cycle in Hybrid Mode at $\beta = 0.85$ (Chassis Dynamometer Test Results)

Table 4.3: MSU HEV Improvements for the UDDS Drive Cycle

Description	Diesel Only	UDDS (β1)	UDDS (β2)	UDDS (β3)
Percentage Improvement over Stock Vehicle (Gasoline Equivalent)	10.84%	7.73%	16.73%	28.84%
Percentage Improvement over Stock Vehicle (SOC Corrected Gasoline Equivalent)	10.84%	25.86%	16.73%	9.00%
Percentage Improvement over Diesel ICE-only configuration (B20 Fuel Economy)	-	-2.82%	5.33%	16.28%
Percentage Improvement over Diesel ICE-only configuration (SOC Corrected B20 Fuel Economy)	-	13.54%	5.33%	-1.67%

Figure 4.15 shows the overall fuel consumption during the UDDS drive cycle for the diesel engine-only configuration and hybrid configuration at the different initial SOCs. It is observed that the fuel consumption in hybrid configuration at an initial SOC of 45% is slightly greater than that in diesel engine-only configuration. The variation of battery SOC during the drive cycle at different initial values are shown in Figure 4.16. The control strategy is able to balance the final SOC at a median level despite varying initial SOC values, thus ensuring charge-sustaining operation during the UDDS drive cycle.

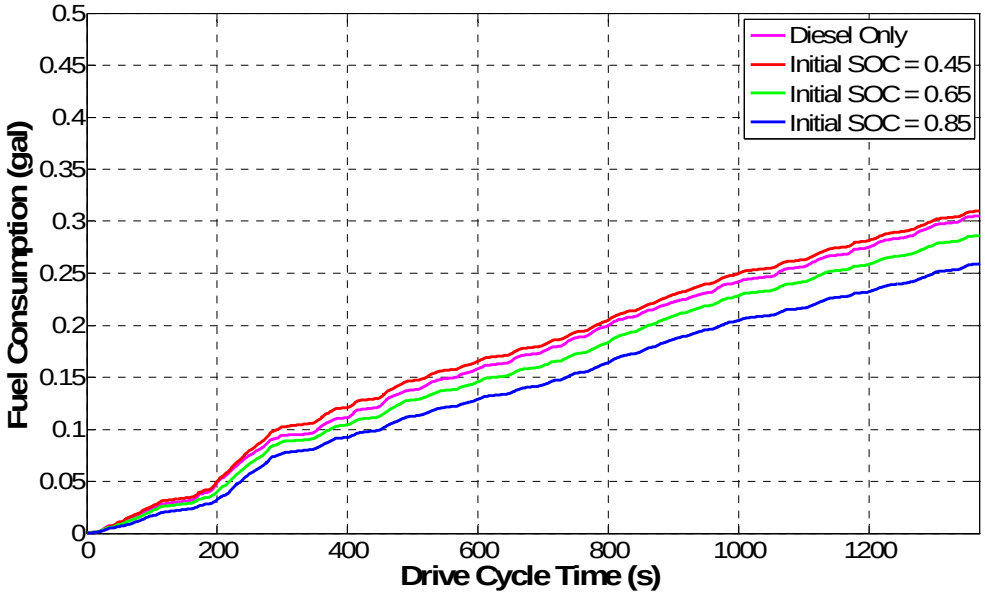

Figure 4.15: Engine Fuel Consumption during UDDS Drive Cycle

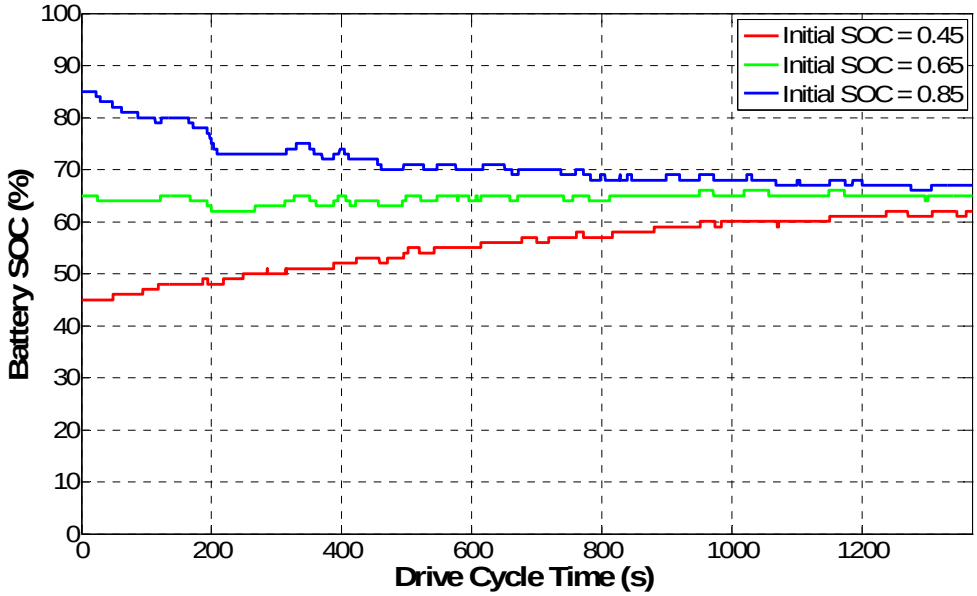

Figure 4.16: Variation of Battery SOC during UDDS for Different Values of β

4.3.3 Highway Fuel Economy Test (HWFET)

Table 4.4 includes RT data from the chassis dynamometer tests for the diesel engine-only and the hybrid configurations during the HWFET drive cycle at the different initial SOCs of 45%, ($\beta_1 = 0.45$), 65% ($\beta_2 = 0.65$) and 85% ($\beta_3 = 0.85$). It is observed that the fuel consumption of the MSU HEV reduces with an increase in initial SOC of the battery. However, the fuel consumption of the diesel-only configuration is the lower than all the hybrid options, thus indicating that it is the most optimal mode of operation. Also, fuel economies during HWFET are higher than the corresponding values during UDDS, since the HWFET does not involve many transient events.

Table 4.4: Chassis Dynamometer Test Results for the HWFET Drive Cycle

Description	HWFET – Diesel Only	HWFET (β1)	HWFET (β2)	HWFET (β3)
Initial SOC	-	0.45	0.65	0.85
Final SOC	-	0.65	0.72	0.76
Fuel Consumed (Gallons)	0.31	0.37	0.32	0.30
B20 Fuel Economy (mi/gal)	33.58	28.21	32.19	33.97
SOC Corrected B20 Fuel Economy (mi/gal)	33.58	32.88	34.13	31.54
Gasoline Equivalent (mi/gal)	28.16	23.66	27.00	28.48
SOC Corrected Gasoline Equivalent (mi/gal)	28.16	27.57	28.62	26.45

Table 4.5 summarizes the improvements made by the diesel-only configuration and the MSU HEV over the stock vehicle. The fuel economy of the stock vehicle during the HWFET as per its technical specifications is 22 mi/gal [23]. Overall, the MSU HEV provides better fuel economy than the stock vehicle. But as anticipated, the diesel engine-only configuration offers a consistent and higher percentage gain in fuel economy over the stock vehicle as compared to the gains offered by the hybridized powertrain at different initial SOCs. In fact, powertrain hybridization leads to reduction in fuel economy over the diesel-only configuration during the HWFET drive cycle.

Table 4.5: MSU HEV Improvements for the HWFET Drive Cycle

Description	Diesel Only	HWFET (β1)	HWFET (β2)	HWFET (β3)
Percentage Improvement over Stock Vehicle (Gasoline Equivalent)	12.64%	-5.36%	8.00%	13.92%
Percentage Improvement over Stock Vehicle (SOC Corrected Gasoline Equivalent)	12.64%	10.28%	14.48%	5.8%
Percentage Improvement over Diesel ICE-only configuration (B20 Fuel Economy)	-	-15.99%	-4.13	1.16%
Percentage Improvement over Diesel ICE-only configuration (SOC Corrected B20 Fuel Economy)	-	-2.08%	1.63%	-6.07%

From Figures 4.17 to 4.20, it is evident that the scatter of engine operating points remains largely concentrated in a region of low engine power output. The HWFET does not involve transient events like those during the UDDS and the most efficient operation is to provide the required load power from the engine alone. This is justified by Figure 4.21 which illustrates that the lowest fuel consumption during the HWFET drive cycle occurs in hybrid mode at an initial SOC of 85% and diesel engine-only mode, respectively. At an initial SOC of 85%, almost negligible battery charging is required and it is quite similar to an engine-only operation. In fact, the electric machine assists the engine in the few acceleration events during the drive cycle.

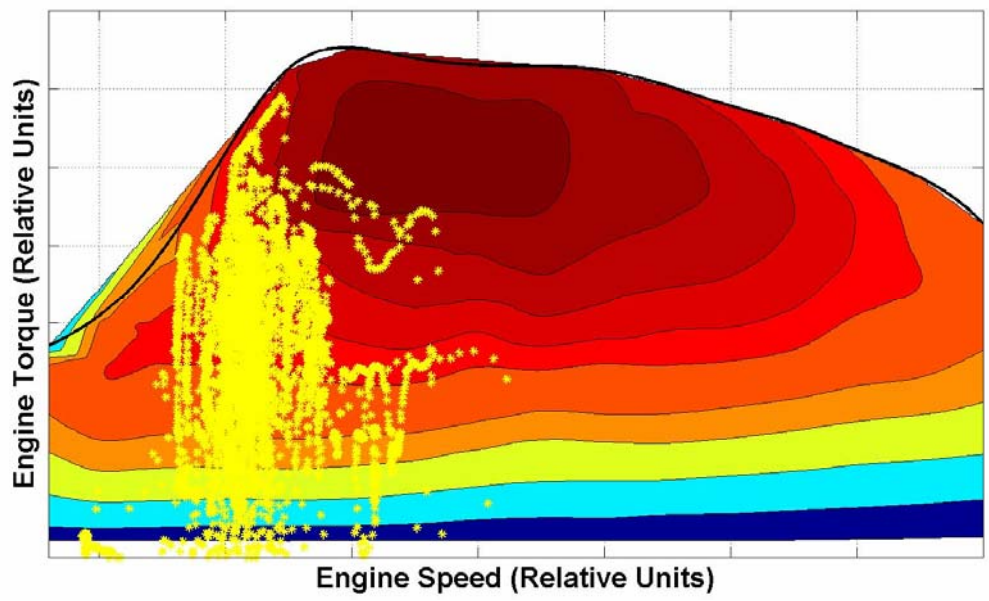

Figure 4.17: Engine Operating Points for the HWFET Drive Cycle in Diesel Engine only Mode (Chassis Dynamometer Test Results)

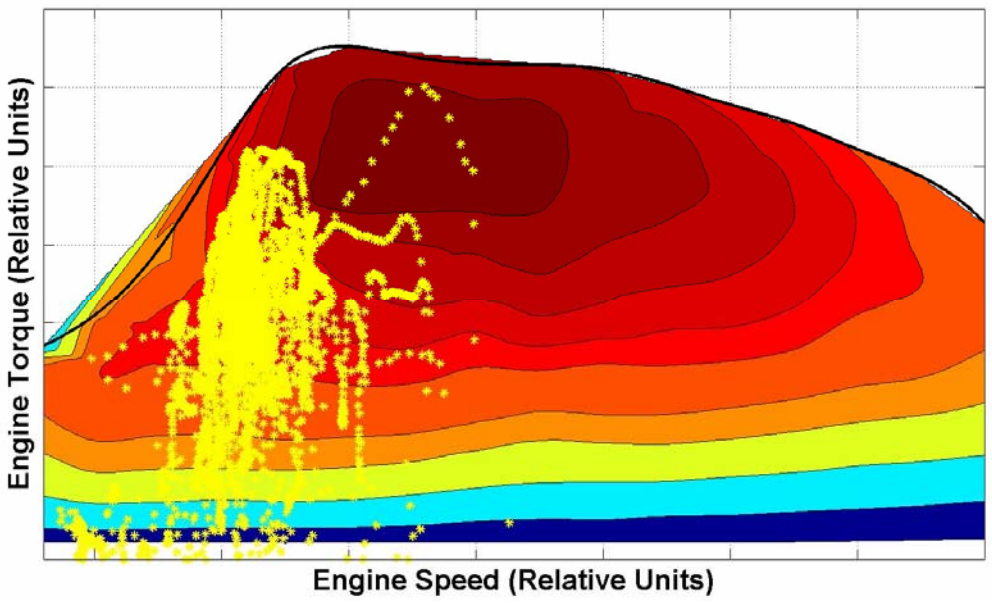

Figure 4.18: Engine Operating Points for the HWFET Drive Cycle in Hybrid Mode at $\beta = 0.45$ (Chassis Dynamometer Test Results)

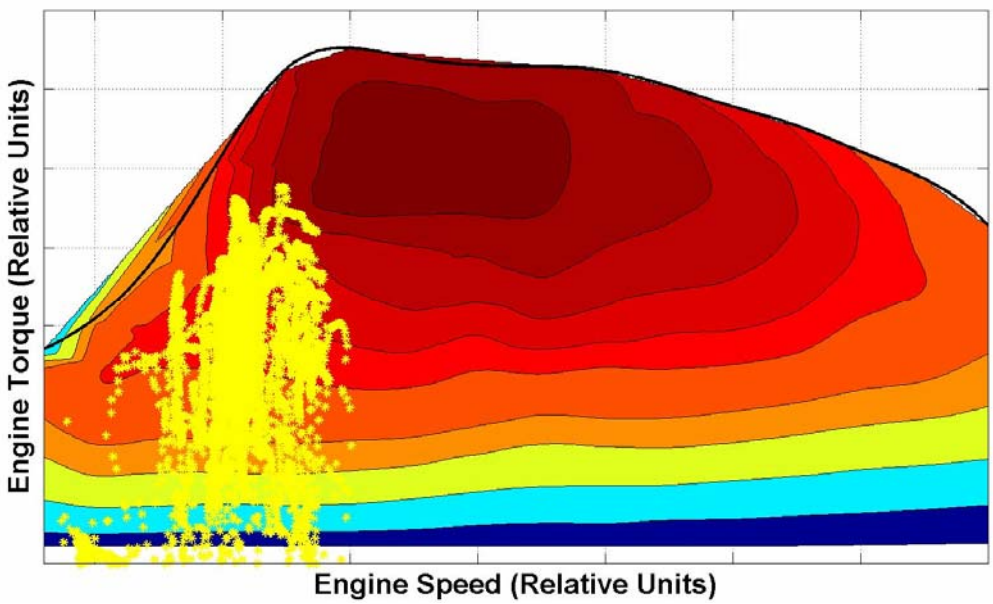

Figure 4.19: Engine Operating Points for the HWFET Drive Cycle in Hybrid Mode at $\beta = 0.65$ (Chassis Dynamometer Test Results)

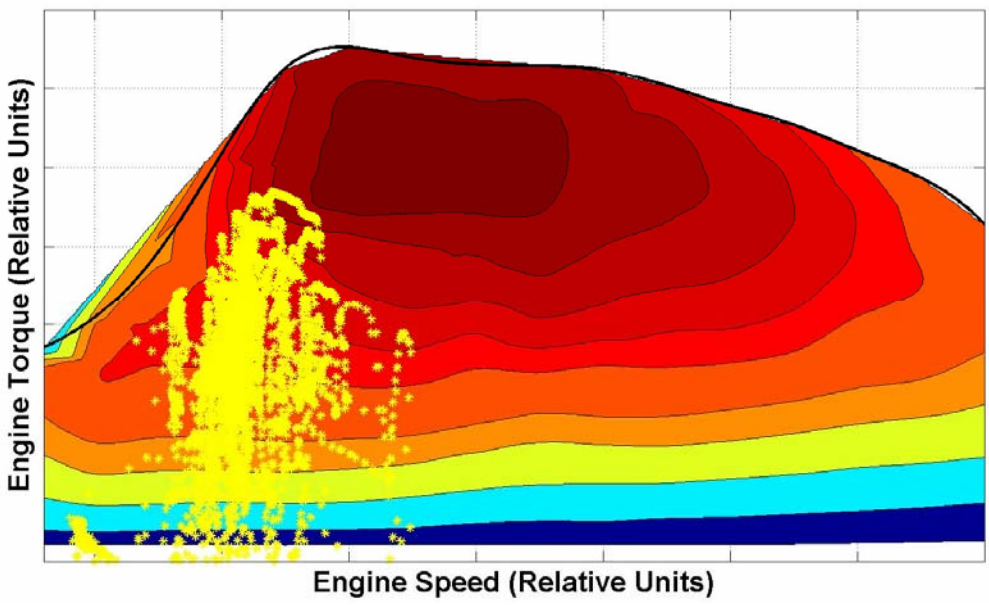

Figure 4.20: Engine Operating Points for the HWFET Drive Cycle in Hybrid Mode at $\beta = 0.85$ (Chassis Dynamometer Test Results)

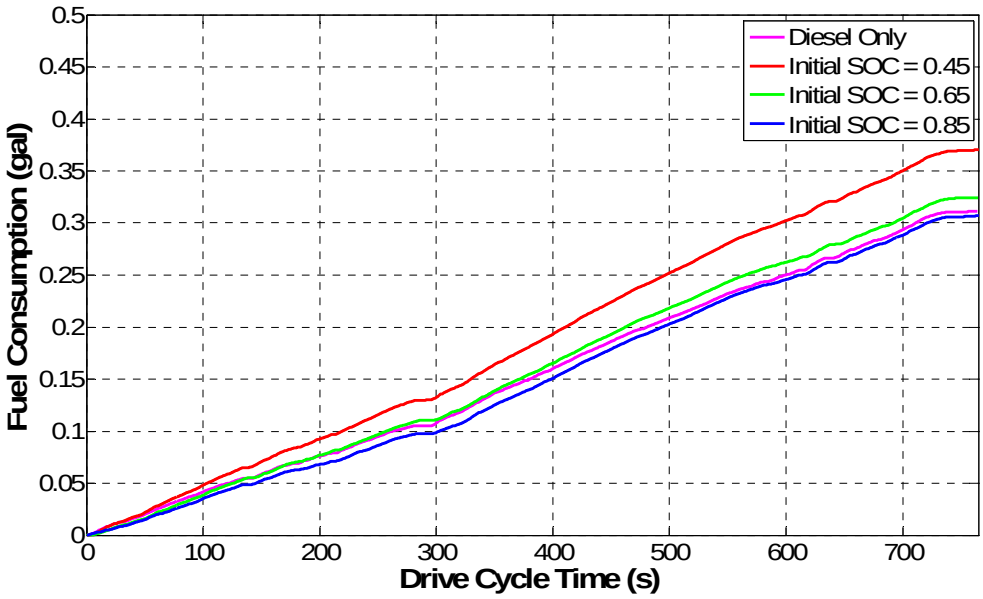

Figure 4.21: Engine Fuel Consumption during HWFET Drive Cycle

At low battery SOCs, light charging of the battery pack leads to greater fuel consumption since the electric machine (operating as a generator) acts as an additional load on the engine. However, charging at low SOCs is significant to ensure battery charge sustainability. The control algorithm successfully maintains the final SOC near or above a median level during the HWFET drive cycle under varying values of β and this is evident from Figure 4.22. In fact at initial SOCs like 65% and 85%, the terminal SOC of the battery is greater than the median level of around 65% and this charging may be detrimental to the overall fuel economy. This is because the electric machine acts as an extra load on the engine and undue battery charging at the expense of B20 biodiesel must be avoided.

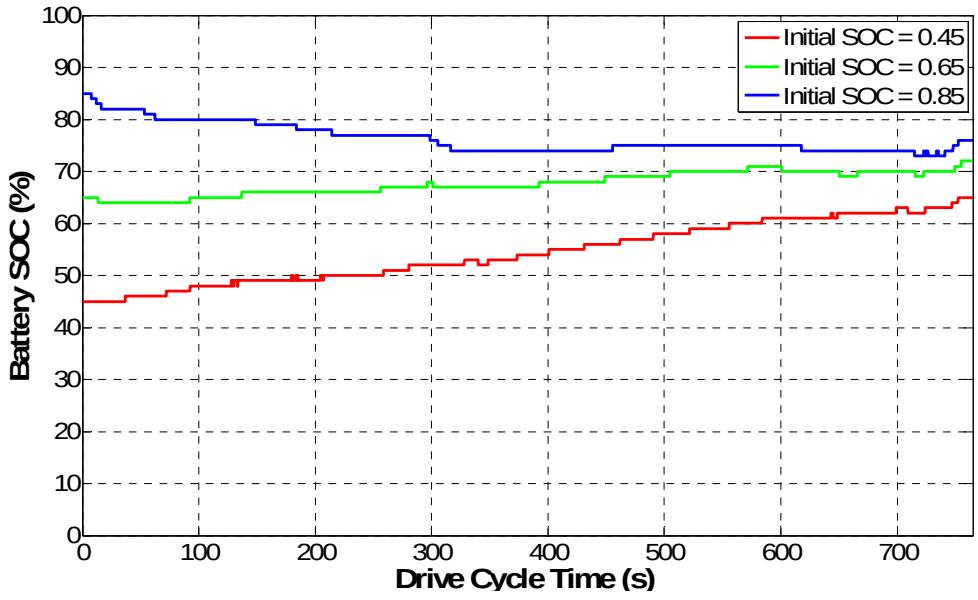

Figure 4.22: Variation of Battery SOC during HWFET for Different Values of β

4.3.4 Federal Test Procedure – 75 (FTP-75)

Table 4.6 displays data from the chassis dynamometer tests for the FTP-75 drive cycle for the diesel engine-only and hybrid configurations at different initial SOCs of 45%, ($\beta_1 = 0.45$), 65% ($\beta_2 = 0.65$) and 85% ($\beta_3 = 0.85$). The average speed of this cycle is greater than that of the UDDS drive cycle and it includes a few more transient events. Despite this, it is interesting to note that the values of B-20 fuel economy (SOC uncorrected) for the FTP-75 drive cycle are greater than the corresponding values for the UDDS drive cycle. The SOC-corrected fuel economies at all values of β are also greater than the corresponding values for the UDDS drive cycle.

Table 4.6: Chassis Dynamometer Test Results for the FTP-75 Drive Cycle

Description	FTP - 75 – Diesel Only	FTP - 75 (β1)	FTP - 75 (β2)	FTP - 75 (β3)
Initial SOC	-	0.45	0.65	0.85
Final SOC	-	0.65	0.65	0.66
Fuel Consumed (gal)	0.43	0.43	0.41	0.38
B20 Fuel Economy (mi/gal)	25.74	25.51	27.19	29.25
SOC Corrected B20 Fuel Economy (mi/gal)	25.74	28.98	27.19	25.89
Gasoline Equivalent (mi/gal)	21.59	21.39	22.80	24.53
SOC Corrected Gasoline Equivalent (mi/gal)	21.59	24.30	22.80	21.70

The scatter of engine operating points for the FTP-75 drive cycle are shown in Figures 4.23 to 4.26. From Figure A.23, it can be observed that there is a slightly denser presence of operating points in the high torque output region of the engine as compared to the UDDS drive cycle. With an increase in the initial SOC of the battery, these high torque points are increasingly shifted to regions of low fuel flow rate thus indicating that the engine unloading strategy is effective during high torque requirements.

The advantages of hybridization and the effectiveness of unloading the engine are evident from Table 4.7 which shows the improvements made by the MSU HEV over a diesel engine-only configuration. Consistent percentage gains in fuel economy are obtained at an initial SOC of 65%.

Table 4.7: MSU HEV Improvements for the FTP-75 Drive Cycle

Description	FTP-75 (β1)	FTP-75 (β2)	FTP-75 (β3)
Percentage Improvement over Diesel ICE-only configuration (B20 Fuel Economy)	-0.89%	5.63%	13.63%
Percentage Improvement over Diesel ICE-only configuration (SOC Corrected B20 Fuel Economy)	12.58%	5.63%	0.58%

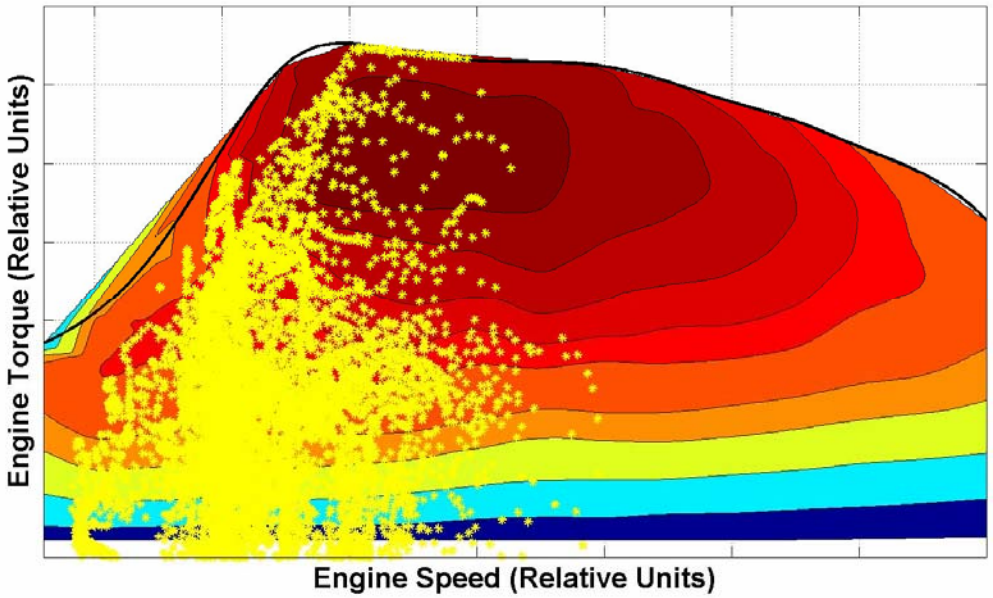

Figure 4.23: Engine Operating Points for the FTP-75 Drive Cycle in Diesel Engine-only Mode (Chassis Dynamometer Test Results)

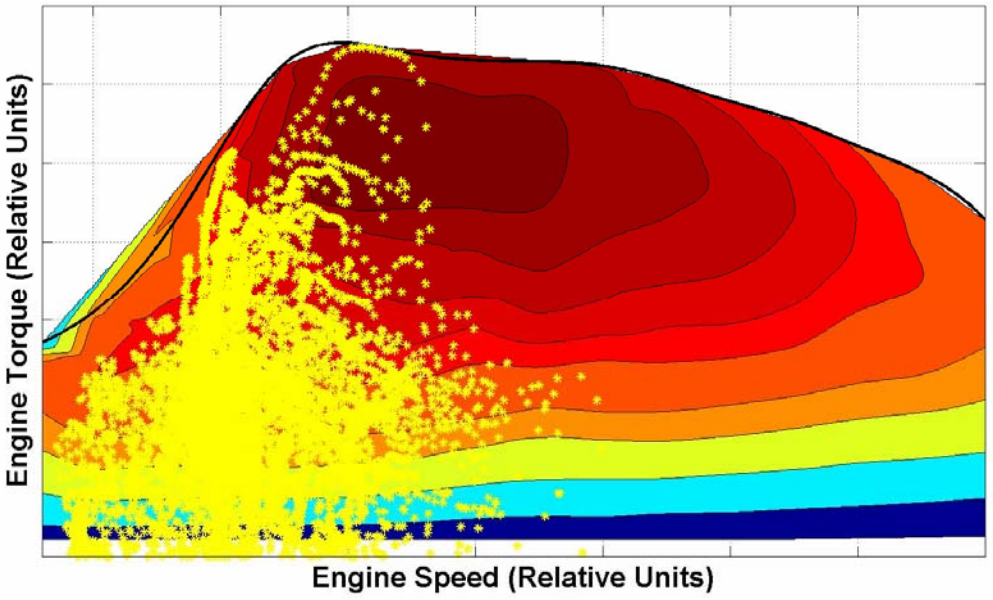

Figure 4.24: Engine Operating Points for the FTP-75 Drive Cycle in Hybrid Mode at $\beta = 0.45$ (Chassis Dynamometer Test Results)

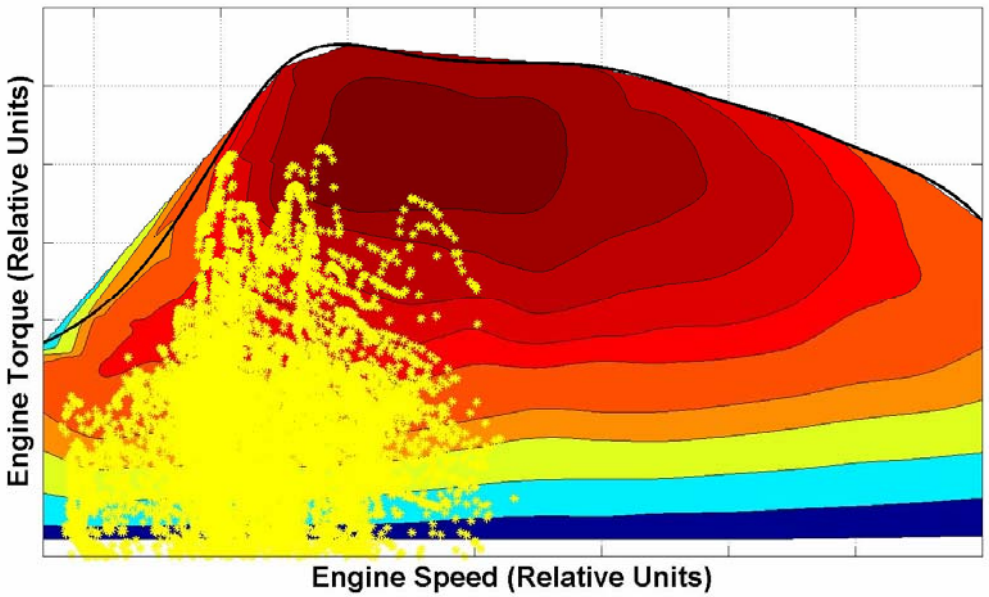

Figure 4.25: Engine Operating Points for the FTP-75 Drive Cycle in Hybrid Mode at β = 0.65 (Chassis Dynamometer Test Results)

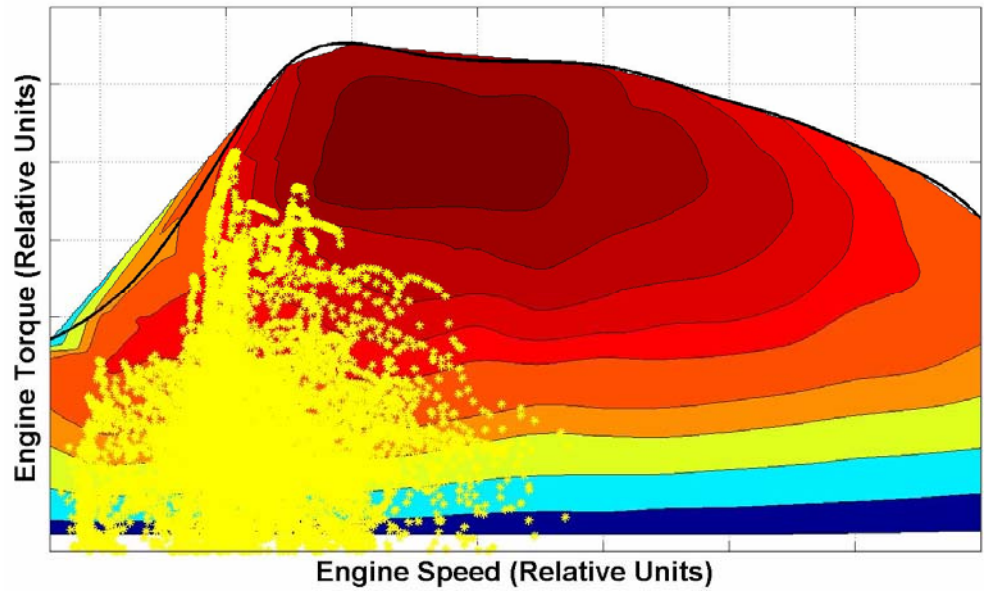

Figure 4.26: Engine Operating Points for the FTP-75 Drive Cycle in Hybrid mode at β = 0.85 (Chassis Dynamometer Test Results)

From Figure 4.27, the fuel consumption for the hybrid configuration at an initial SOC of 45% at the end of the FTP-75 drive cycle is almost same as that for the diesel engine-only configuration. This indicates that at low SOCs the electric machine does provide limited torque assist. Significant reduction in fuel consumption is obtained at higher values of initial SOC where more torque assist is provided. From Figure 4.28, it is evident that the control strategy successfully balances the final SOC at a median value under all varying conditions of initial SOC, thus ensuring charge-sustainability during the FTP-75 drive cycle.

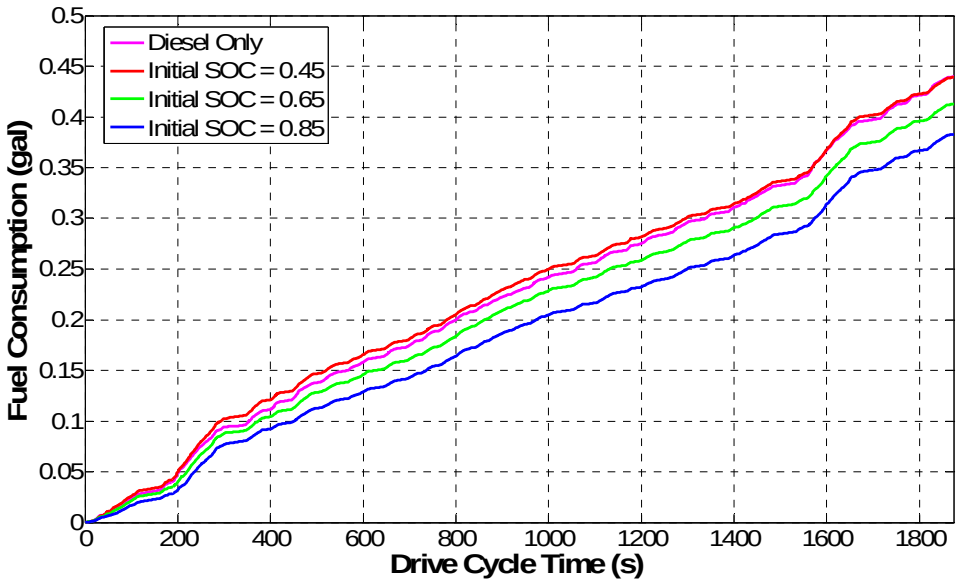

Figure 4.27: Engine Fuel Consumption during FTP-75 Drive Cycle

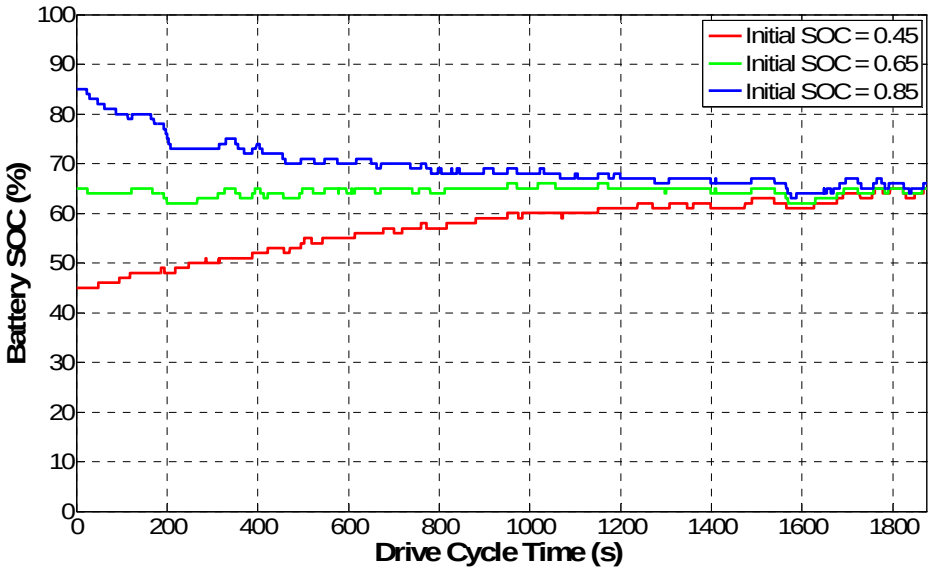

Figure 4.28: Variation of Battery SOC during FTP-75 for Different Values of β

4.3.5 US06 Supplemental Federal Test Procedure (US06 SFTP)

Table 4.8 displays data from the chassis dynamometer tests during the US06 drive cycle for the diesel-only and the hybrid configurations at different initial SOCs of 45%, (β_1 = 0.45), 65% (β_2 = 0.65) and 85% (β_3 = 0.85). The most consistent and largest percentage gains in fuel economy due to powertrain hybridization are obtained for this drive cycle. This is despite the fact that values of fuel economy are numerically the lowest for this drive cycle due to its aggressive speed profile.

The benefits of powertrain hybridization for the US06 are amply demonstrated from the gains obtained over a diesel engine-only configuration and these are enumerated in Table 4.9. The MSU HEV achieves a gain in fuel economy over a diesel-only configuration at virtually all values of initial SOC.

Table 4.8: Chassis Dynamometer Test Results for the US06 Drive Cycle

Description	US06 – Diesel Only	US06 (β1)	US06 (β2)	US06 (β3)
Initial SOC	-	0.45	0.65	0.85
Final SOC	-	0.54	0.61	0.63
Fuel Consumed (gal)	0.34	0.33	0.30	0.28
B20 Fuel Economy (mi/gal)	23.49	24.22	26.35	28.65
SOC Corrected B20 Fuel Economy (mi/gal)	23.49	26.06	25.48	23.79
Gasoline Equivalent (mi/gal)	19.70	20.31	22.10	24.02
SOC Corrected Gasoline Equivalent (mi/gal)	19.70	21.86	21.37	19.95

Table 4.9: MSU HEV Improvements for the US06 Drive Cycle

Description	US06 (β1)	US06 (β2)	US06 (β3)
Percentage Improvement over Diesel ICE-only configuration (B20 Fuel Economy)	3.11%	12.18%	21.97%
Percentage Improvement over Diesel ICE-only configuration (SOC Corrected B20 Fuel Economy)	10.94%	8.47%	1.28%

From Figures 4.29 to 4.32, it is evident that the US06 is the most aggressive of all the drive cycles with high load power requirements. There is a visible shift in the scatter of engine operating points to regions of low fuel flow rate with an increase in the SOC of the battery, thereby emphasizing the role of electric machine in unloading the engine.

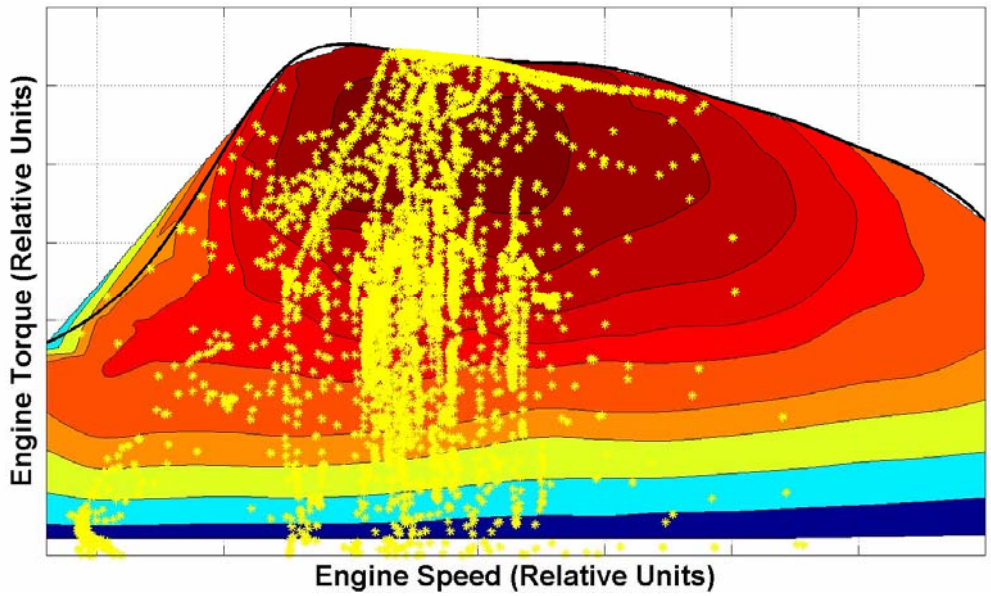

Figure 4.29: Engine Operating Points for the US06 Drive Cycle in Diesel Engine-only Mode (Chassis Dynamometer Test Results)

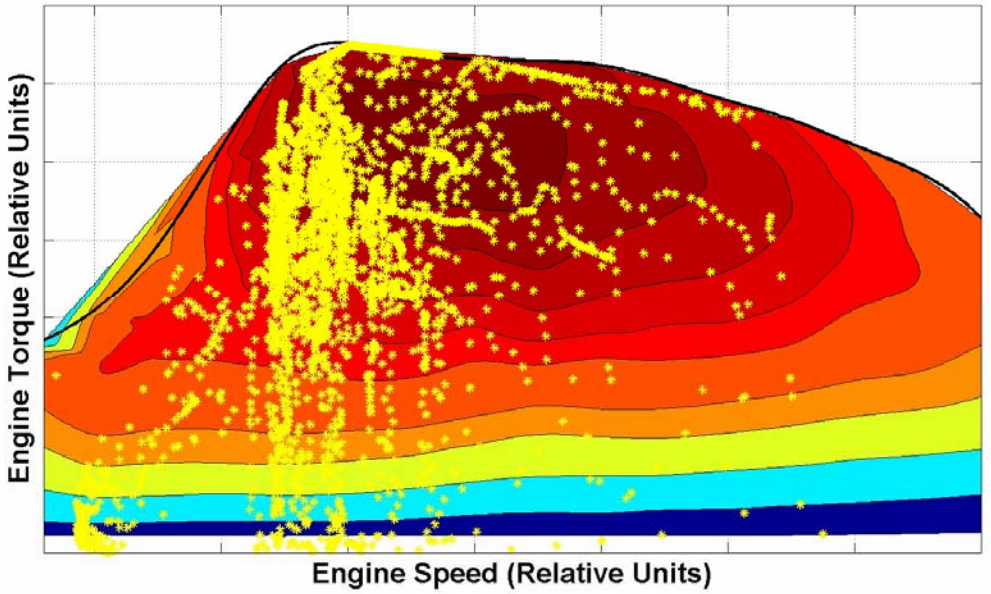

Figure 4.30: Engine Operating Points for the US06 Drive Cycle in Hybrid Mode at $\beta = 0.45$ (Chassis Dynamometer Test Results)

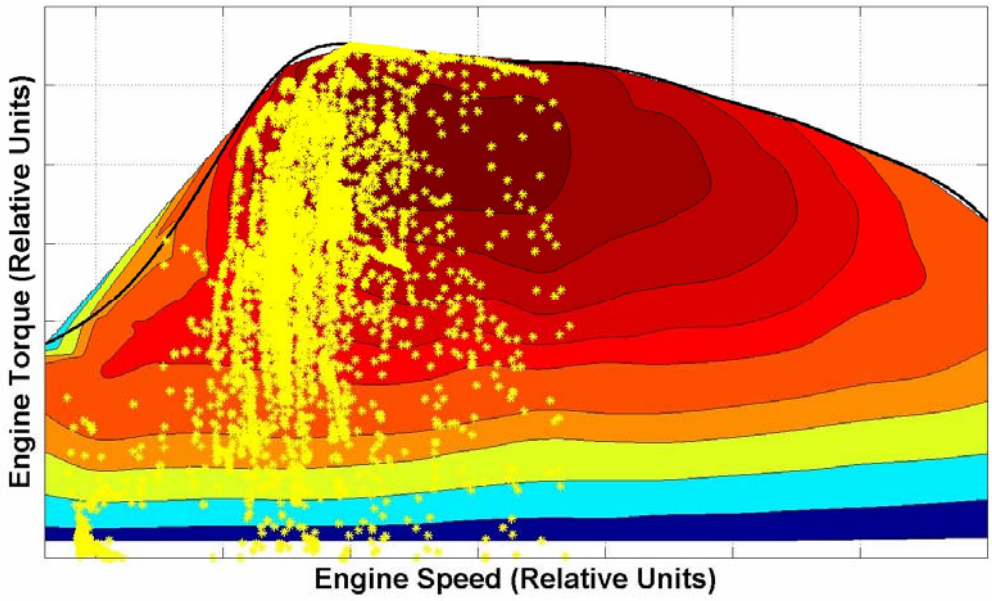

Figure 4.31: Engine Operating Points for the US06 Drive Cycle in Hybrid Mode at β = 0.65 (Chassis Dynamometer Test Results)

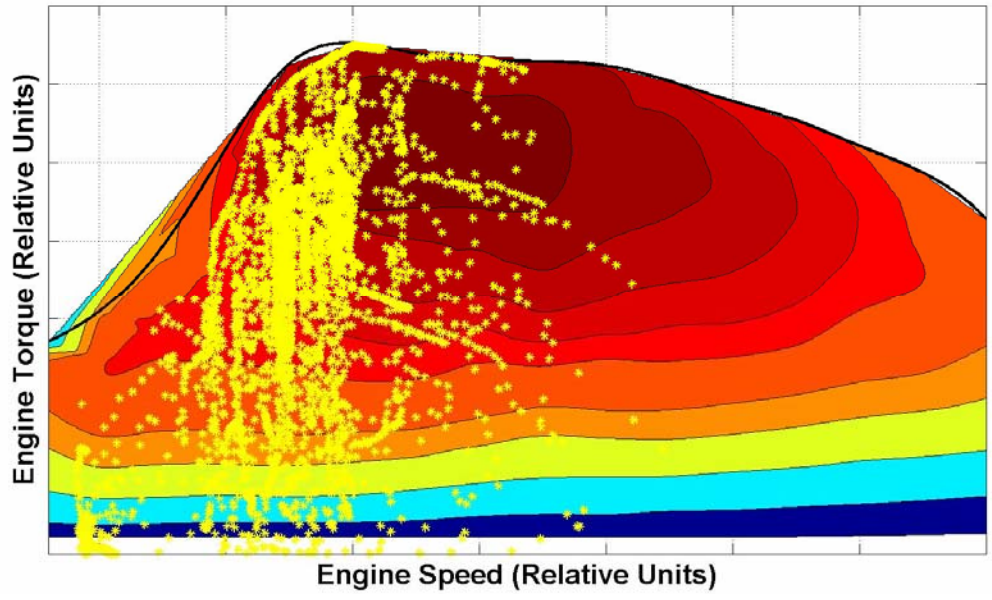

Figure 4.32: Engine Operating Points for the US06 Drive Cycle in Hybrid Mode at β = 0.85 (Chassis Dynamometer Test Results)

Figure 4.33 displays a clear trend of reduced fuel consumption in hybrid configurations over the diesel engine-only configuration. This reduction in fuel consumption is more pronounced at higher initial SOCs of the battery thus suggesting that during aggressive drive cycles, engine unloading by increased use of electric machine is very effective for reducing overall fuel consumption. The control strategy successfully maintains the battery SOC at a median level under varying values of initial SOC. This is illustrated in Figure 4.34 and is a good indication of the effectiveness of the control strategy in maintaining charge-sustainability despite the aggressive nature of the cycle.

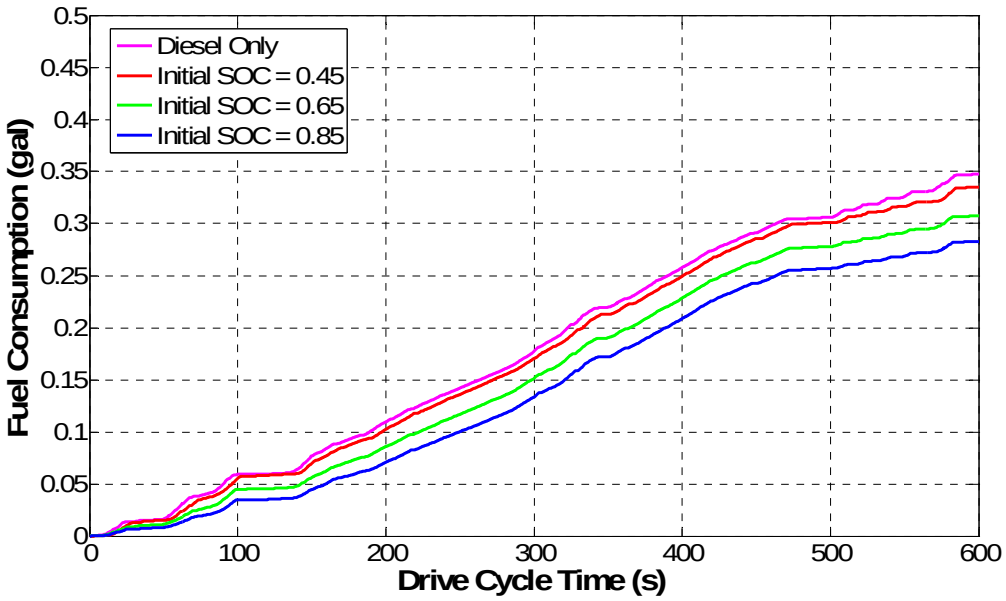

Figure 4.33: Engine Fuel Consumption during US06 Drive Cycle

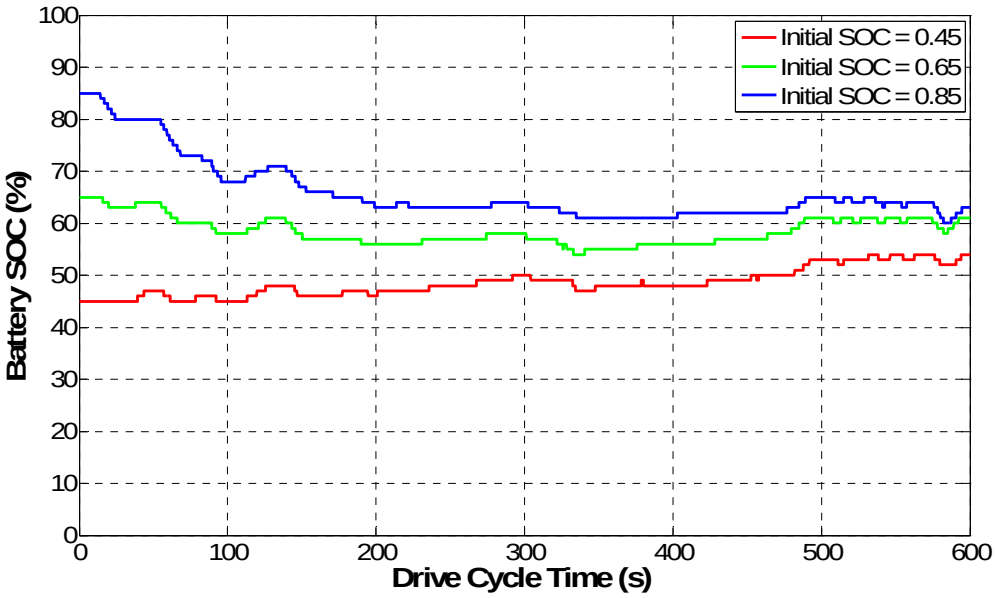

Figure 4.34: Variation of Battery SOC during US06 for Different Values of β

CHAPTER 5

CONCLUSIONS AND FUTURE WORK

5.1 Conclusions

This thesis presents the development and validation of a powertrain-level control strategy for a diesel-electric TTR parallel HEV. The benefits of powertrain hybridization have been analyzed for the gains obtained over the stock gasoline vehicle. Additionally, the performance of the hybrid configuration has been evaluated for its effectiveness over a diesel engine-only configuration over several diverse drive cycles. While there are many degrees of freedom for control of an HEV, this study focuses on reducing the instantaneous fuel flow rate to the engine. This is achieved by indirectly unloading the engine through use of the electric machine and thus attempting to operate in regions of low instantaneous fuel-flow rates and low NO_X emissions.

Fuel consumption is a direct function of the load point of an engine. Fuel consumption is also dependant on many other factors like engine design, aerodynamics, vehicle weight, drive cycle, driver behavior etc. [22]. Assuming a constant effect due to all other factors, the load power requirements of a drive cycle have a clear impact on the effectiveness of the developed control strategy. The UDDS drive cycle, for example, represents urban driving at low vehicle speeds and it leads to low engine loads. In view of the low load power requirements, the engine unloading strategy is not very effective,

especially at low battery SOCs. While the FTP-75 drive cycle traces the UDDS for a major portion of time, it includes some additional operating points of high engine torque requirement. The control strategy is more effective during the FTP-75 where the electric machine helps unload the engine during a larger portion of drive cycle time.

Highway driving clearly highlights the difference in the performance of the control strategy. During the HWFET drive cycle, either the diesel engine-only configuration or hybrid configuration at a high battery SOC provide best performance. The benefits of powertrain hybridization are not evident for low battery SOCs. However, during the US06 drive cycle, which has a comparable average speed as the HWFET and includes a substantial portion of cruising at high speeds and more aggressive accelerations, the HEV powertrain offers consistent benefits over a diesel engine-only configuration at all levels of battery SOCs. The effectiveness of unloading the engine is thus more prominent during drive cycles that require high load power.

The ability to be charge-sustaining is an important expectation from the powertrain control strategy. The property of charge recovery and sustainability has been validated over several driving schedules and at different initial SOCs. Data to this effect have been illustrated in Chapter 4. The control strategy maintains the SOC at a median level regardless of the initial SOC, during all the considered drive cycles. Thus hybrid control strategies cannot merely take into account the general energy flow in the powertrain, but they also have to account for other powertrain requirements. Overall, the developed control strategy meets the objectives and minimum performance targets to be achieved.

5.2 Future Work

Limiting dynamic operation of the engine is beneficial because it is often argued that in contrast to steady-state operation, the engine consumes fuel and generates emissions out of proportion when changes in operating points occur above a certain rate [22]. In the developed control strategy, no efforts have been made to limit any transient operation of the engine that may occur. It has been suggested that quasi-stationary operation of the engine can be induced by introducing a low pass filter with an appropriate time constant to filter the power requested [22]. Alternatively, it is worthwhile to investigate the improvements that may be obtained by introduction of engine load-leveling in the control strategy. This will effectively mean that the original bias between the accelerator pedal and engine ECU may have to be altered. The engine can be forced to operate at steady/constant optimum power levels depending on the required load power and the electric machine can be made to supply the transient power requirements. This may also facilitate investigation of an engine-efficiency optimization control strategy.

Substantial improvements may be possible by limiting the battery charging above a certain SOC. This can be especially significant during highway driving schedules where the electric machine is an additional load on the engine.

5.3 Evaluation of Engine Load-leveling in the MSU HEV

The underlying idea of engine load-leveling strategy is to force the engine to operate at high efficiencies. The GM diesel engine in the MSU HEV configuration has a peak efficiency of about 39%. The power output in this region is around the magnitude of

60 kW. This is region A in Figure 5.1. During common drive cycles like the UDDS and the HWFET the engine operating points are largely concentrated in regions of power output between 15 kW and 30 kW (region B). This is evident from the chassis dynamometer tests for the diesel engine-only configuration. The engine efficiency in region B is typically between 31% and 35%. An important point to note is that the ratio of engine fuel flow rate in region A to that in region B is approximately 3:1 at each time instance. This effectively means that although the engine can operate at its peak efficiency in region A, it will consume about 3 times more fuel than in region B.

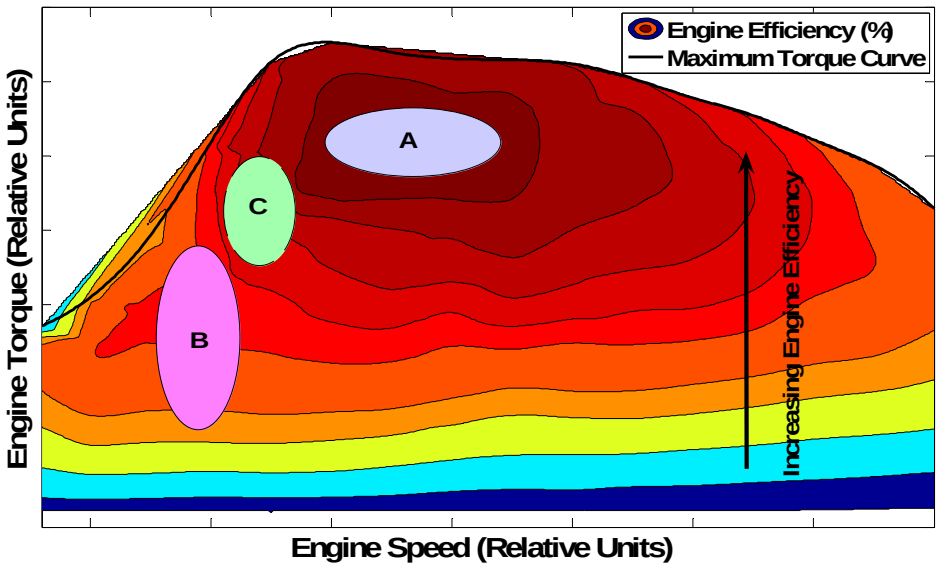

Figure 5.1: Evaluation of Engine Load-leveling for the 1.9 L GM Diesel Engine

In drive cycles like the UDDS and the HWFET, the road load demand is not too high and hence high power output is not warranted from the engine. If the engine is forced to operate in region A, the additional fuel consumed by the engine (and hence the

output power produced) may not always be effectively converted into electrical power to charge the battery at all times. This is because, despite consistently operating the engine at a high efficiency, the physical limitations associated with the battery, will limit charging beyond a certain extent. Thus, the feasibility of converting the 'high-efficiency', power output of the engine into electric power in order to store energy is debatable, since any gains in engine operating efficiency are offset by an accompanying rise in fuel flow to the engine and the resulting power output may not always be used to the optimum.

For a marginal gain in engine efficiency, it may not be worthwhile to pursue the engine load-leveling strategy at the expense of a multi-fold increase in fuel flow, unless the road load demand necessitates engine operation in region A. However, in drive cycles like UDDS that involve substantial transient operation, a better strategy would be to operate the engine at a constant power level, say 45 kW (region C). The electric machine can be used to account for any transient power requirements. This scheme will ensure reasonable engine efficiency (about 37%) without any undue increase in the fuel flow rate to the engine (approximately 1.5 times).

REFERENCES

[1] M. Ehsani, Y. Gao, S. E. Gay, and A. Emadi, *Modern Electric, Hybrid Electric, and Fuel Cell Vehicles: Fundamentals, Theory, and Design*, Washington D.C.: CRC Press, 2004, ch. 5, ch. 8.

[2] H. Wallentowitz, and R. Ludes, "System control application for hybrid vehicles," *Proc. 3rd IEEE Conference Control Applications*, vol. 1, pp. 639-650, August 1994.

[3] Hybrids Under the Hood [Online]. Available : http://www.hybridcenter.org/hybrid-center-how-hybrid-cars-work-under-the-hood.html

[4] A. Rault, "Mid and long term powertrains evolution associated fuels," presented at the European Council for Automotive R&D (EUCAR), February 2002.

[5] D. Friedman. (2003, January). A New Road: The Technology and Potential of Hybrid Vehicles, Union of Concerned Scientists. [Online]. Available : http ://www.ucsusa.org/assets/documents/clean_vehicles/Hybrid2003_final.pdf

[6] Ford Concept Micro Hybrid [Online]. Available: http://www.greencarcongress.com/2004/09/ford_concept_mi.html

[7] J. M. Miller, *Propulsion Systems for Hybrid Vehicles*, London: The Institution of Electrical Engineers, 2004, ch. 3.

[8] J. C. Mathews, K. J. Walp, and G. M. Molen, "Development and implementation of a control system for a parallel hybrid powertrain," *Proc. 2006 IEEE Vehicle Power and Propulsion Conference*, Windsor, September 2006, to be published.

[9] F. Salmasi, "Designing control strategies for hybrid electric vehicles," presented at IASTED International Conference on Applied Simulation and Modeling, June 2005.

[10] L. Sapronov, "Control system design and simulation for the Corona HEV – Cornell University's entry in the Future Truck challenge," presented at the MathWorks International Automotive Conference, June 2003.

[11] K. Bailey, S. Cikanek and N. Sureshbabu, "Parallel hybrid electric vehicle torque distribution method," *Proc. 2002 American Control Conference*, vol. 5, pp. 3708-3712, May 2002.

[12] B. M. Baumann, G. Washington, B. C. Glenn, and G. Rizzoni, "Mechatronic design and control of hybrid electric vehicles," *IEEE/ASME Trans. Mechatronics*, vol. 5, no. 1, pp. 58-72, March 2000.

[13] A. Rousseau, *Description of Control Strategies*, PSAT 5.2 Documentation, Argonne National Laboratory, 2004.

[14] C. Liang, W. Qingnian, L. Youde, M. Zhimin, Z. Ziliang, and L. Di, "Study of the electronic control strategy for the power train of hybrid electric vehicle," *Proc. IEEE International Vehicle Electronics Conference*, vol. 1, pp. 383-386, September 1999.

[15] D. L. Buntin, and J. W. Howze, "A switching logic controller for a hybrid electric/ICE vehicle," *Proc. 1995 American Control Conference*, vol. 2, pp. 1169-1175, June 1995.

[16] T. Ciccarelli, and R. Toossi, "Assessment of hybrid configuration and control strategies in planning future metropolitan/urban transit systems," METRANS Transportation Center, California State University Long Beach, May 2002.

[17] N. Jalil, N. A. Kheir, and M. Salman, "A rule-based energy management strategy for a series hybrid vehicle," *Proc. 1997 American Control Conference*, vol. 1, pp. 689-693, June 1997.

[18] Z. Rahman, K. L. Butler, and M. Ehsani, "A comparison study between two parallel hybrid control concepts," *SAE 2000 World Congress*, SAE Paper No. 2000-01-0994, March 2000.

[19] D. Choi, M. Im, and H. Kim, "An operation algorithm with state of charge recovery for a parallel-type hybrid vehicle," *Proc. of the Institution of Mechanical Engineers*, Part D, Journal of Automobile Engineering, vol. 217, no. 9, pp. 801-807, September 2003.

[20] R. Guyton, et al., "Design and development of the Georgia Tech 2003 Model GT split-parallel hybrid-electric FutureTruck" submitted to 2003 FutureTruck organizers, May 2003.

[21] J. Meisel, "An analytic foundation for the Toyota Prius THS-II powertrain with a comparison to a strong parallel hybrid electric powertrain," *SAE 2006 World Congress*, SAE Paper No. 2006-01-0666, March 2006.

[22] K. Jonasson, "Control of Hybrid Electric Vehicles with Diesel Engines," Doctoral Dissertation, Department of Industrial Electrical Engineering and Automation, Lund University, Sweden, 2005.

[23] 2005 Chevrolet Equinox specifications [Online]. Available: http://media.gm.com/division/2005_prodinfo/chevrolet/trucks/equinox/specifications.htm

[24] Challenge X: crossover to sustainable mobility [Online]. Available: http://www.challengex.org

[25] V. H. Johnson, K. B. Wipke, and D. J. Rausen, "HEV control strategy for real-time optimization of fuel economy and emissions," *Proc. of the Future Car Congress*, SAE Paper No. 2000-01-1543, April 2000.

[26] K. Aoki, S. Kuroda, S. Kajiwara, H. Sato, and Y. Yamamoto, "Development of Integrated Motor Assist hybrid system: development of the 'Insight', a personal hybrid coupe," presented at Government/Industry Meeting, SAE Paper No. 2000-01-2216, June 2000, Washington, DC.

[27] *Operational diagram for NiMH battery*, VARTA Automotive Systems GmbH.

[28] G. Bower, and M. Koplin, "Hybrid brake system," U. S. Patent 6,231,135 B1, May 15, 2001.

[29] R. F. Rowe, J. A. Topinka, E. K. Brodsky, J. G. Marshaus, and G. R. Bower "Design and optimization of the University of Wisconsin's parallel hybrid electric sport utility vehicle," submitted to 2001 FutureTruck organizers, May 2001.

[30] T. Markel, A. Brooker, et al., "ADVISOR: A systems analysis tool for advanced vehicle modeling," *Journal of Power Sources*, vol. 110, pp. 255-266, 2002.

[31] A. Rousseau, S. Saglini, M. Jakov, D. Gray, and K. Hardy, "Trade-offs between fuel economy and NO_X emissions using fuzzy logic control with a hybrid CVT configuration," *International Journal of Automotive Technology*, vol. 4, no. 1, pp. 47-55, 2003.

[32] Testing and measuring emissions [Online]. Available : http://www.epa.gov/OMS/labda.htm#vehcycles

[33] Emission test cycles [Online]. Available: http://www.dieselnet.com/standards/cycles/

[34] Battery open-circuit voltage estimation by a method of statistical analysis [Online]. Available: http://www.eurandom.tue.nl/reports/2005/046ISreport.pdf

APPENDIX A

PSAT SIMULATION RESULTS

Table A.1: PSAT Simulation Results for the UDDS Drive Cycle

Description	UDDS (β1)	UDDS (β2)	UDDS (β3)
Initial SOC	0.45	0.65	0.85
Final SOC	0.65	0.66	0.69
Fuel Consumed (gal)	0.22	0.20	0.17
B20 Fuel Economy (mi/gal)	32.22	36.74	41.44
SOC Corrected Gasoline Equivalent (mi/gal)	35.49	31.99	28.91

Table A.2: PSAT Simulation Results for the HWFET Drive Cycle

Description	HWFET (β1)	HWFET (β2)	HWFET (β3)
Initial SOC	0.45	0.65	0.85
Final SOC	0.74	0.79	0.86
Fuel Consumed (gal)	0.32	0.30	0.27
B20 Fuel Economy (mi/gal)	31.12	33.88	37.71
Gasoline Equivalent (mi/gal)	26.43	28.77	32.02
SOC Corrected Gasoline Equivalent (mi/gal)	34.07	32.97	32.65

Table A.3: PSAT Simulation Results for the FTP-75 Drive Cycle

Description	FTP - 75 (β1)	FTP - 75 (β2)	FTP - 75 (β3)
Initial SOC	0.45	0.65	0.85
Final SOC	0.67	0.68	0.69
Fuel Consumed (gal)	0.32	0.29	0.27
B20 Fuel Economy (mi/gal)	33.32	36.54	39.85
Gasoline Equivalent (mi/gal)	28.29	31.03	33.84
SOC Corrected Gasoline Equivalent (mi/gal)	34.45	32.03	29.71

Table A.4: PSAT Simulation Results for the US06 Drive Cycle

Description	US06 (β1)	US06 (β2)	US06 (β3)
Initial SOC	0.45	0.65	0.85
Final SOC	0.68	0.72	0.76
Fuel Consumed (gal)	0.30	0.27	0.26
B20 Fuel Economy (mi/gal)	26.26	28.67	30.81
Gasoline Equivalent (mi/gal)	22.30	24.35	26.16
SOC Corrected Gasoline Equivalent (mi/gal)	27.81	26.13	24.09

APPENDIX B

CALCULATIONS FOR STATE OF CHARGE CORRECTION AND GASOLINE EQUIVALENT FUEL ECONOMY

The operational cost of an HEV in any driving scenario can be expressed as the sum of the cost of fossil fuel (B20 bio-diesel for the MSU HEV) consumed by the engine and the cost of electricity consumed by the electric machine during a unit time interval. An ideal charge-sustaining control strategy should account for the cost of using the electric machine to exchange energy from the battery as well as the cost of using the engine to consume energy from the fossil fuel. The electric machine in a parallel hybrid system operates either as a generating device or as a traction device. The battery is either supplied with electric charge (regeneration) or is discharged (traction). In order to maintain a balanced SOC level during a drive cycle, any electric charge removed from the battery or added into the battery must be accounted for in the calculations for fuel economy. This is done by means of an SOC correction factor which is defined as an SOC-related coefficient that is used to scale the energy consumed or produced by the electric machine [10, 19, 25].

When there is a difference in the amount of charge moving in and out of the battery, the SOC of the battery at the end of the drive cycle will be different from that at the start of the drive cycle. The change in SOC (ΔSOC) is accounted based on the equivalent amount of fossil fuel it represents. The term ΔSOC could represent either depletion or enhancement of the battery SOC, and in either case the SOC needs to be restored to its initial SOC level while calculating the fuel economy of the HEV. This is done by calculating a ΔSOC-equivalent of fossil fuel energy. This equivalent energy is a hypothetical energy and its computation involves energy conversion efficiencies of the engine, the electric machine and the battery along with temperature-related performance

factors. It is not straightforward to account for inefficiencies due to exchanging electrical energy with the battery pack. In this document, the conversion from the fossil fuel energy to electrical energy is assumed to occur at a fixed efficiency of 25%. Also, the open circuit voltage (V_{OC}) of a battery pack is a function of the SOC and this function is expected to remain the same during the battery lifetime. However, other critical battery characteristics like the battery capacity change with time and operating temperature thereby affecting V_{OC} estimation [34]. With a view to simplify calculations, the V_{OC} for this battery pack is assumed to be equal to a nominal value of 350 V.

The procedure adopted for calculation of different SOC-corrected economies of the MSU HEV is discussed below. This is based on the method adopted at the cX competition. Definitions of the variables used have been listed in the List of Symbols. Values of the constants used are given below. It is assumed that battery power is negative for discharging and positive for charging.

E_{B20} = Specific energy content of bio-diesel (B20) = 127,259 BTU/gal

E_{RFG} = Specific energy content of reformulated gasoline (RFG) = 106,720 BTU/gal

C = Capacity of the JCI NiMh battery pack = 7 A-h

V_{NOCV} = Nominal open circuit voltage of the battery pack = 350 V

η_{CON} = Cumulative conversion efficiency = 25%

The simple fuel economy of the HEV is given as the ratio of distance traveled to the amount of B20 bio-diesel used.

$$B20FuelEconomy(mi/gal) = \frac{d}{\gamma} \tag{6}$$

The difference in electrical energy levels (kW-h) of the battery pack due to any change in final and initial SOC (A-h) of the battery pack is then computed. A negative difference indicates that the SOC at the end of the cycle is less than the initial SOC.

$$\Delta SOC(Ah) = \frac{(\lambda - \beta)}{100} \times c \tag{7}$$

$$\Delta SOC(kWh) = \frac{\Delta SOC(Ah) \times V_{NOCV}}{1000} \tag{8}$$

Assuming a conversion efficiency of 25%, the change in electrical energy (kW-h) is converted to the corresponding heating value or energy content of the fossil fuel (BTU), i.e. B20 bio-diesel. This value indicates how much fossil fuel must be expended to account for the difference in SOC of the battery pack.

1 kW = 3412 BTU/h

$$E_{IN}(BTU) = -\frac{\Delta SOC(kWh)}{\eta_{CON}} \times 3412 \tag{9}$$

The heating value of B20 bio-diesel actually used by the engine is then computed.

$$E_{OUT}(BTU) = E_{B20} \times \gamma \tag{10}$$

The cumulative energy content of the fossil fuel used by the HEV is then divided by the distance traveled to determine the energy consumption per mile traveled while simultaneously maintaining a constant SOC.

$$E_{CUM}(BTU/mi) = \frac{[E_{IN}(BTU) + E_{OUT}(BTU)]}{d} \tag{11}$$

Knowing the specific energy content of B20 bio-diesel, the SOC corrected fuel economy of the HEV can be computed as follows.

$$SOC\_Corrected\_B20FuelEconomy(mi/gal) = \frac{E_{B20}(BTU/gal)}{E_{CUM}(BTU/mi)} \quad (12)$$

The stock vehicle is equipped with a gasoline engine. Due to the difference in energy contents of RFG and B20 bio-diesel, it is imperative to compare the improvements over the stock configuration on a common scale. For this purpose the fuel economy obtained by use of B20 bio-diesel is converted to its gasoline equivalent (GE) value using the following equations. Knowing the specific energy content of RFG, the gasoline equivalent fuel economy in mi/gal (without SOC correction) is given by Equation 13.

$$FuelEconomy\_GE(mi/gal) = B20FuelEconomy(mi/gal) \times \frac{E_{RFG}(BTU/gal)}{E_{B20}(BTU/gal)} \quad (13)$$

SOC correction can also be factored into the gasoline equivalent fuel economy. Equation 14 describes calculation of the SOC corrected, gasoline equivalent value of fuel economy.

$$SOC\_Corrected\_GEFuelEconomy(mi/gal) = \frac{E_{RFG}(BTU/gal)}{E_{CUM}(BTU/mi)} \quad (14)$$